Morphological analysis of stylolites for paleostress estimation in limestones surrounding the Andra Underground Research Laboratory site

Rolland A.[(a,b)*], R. Toussaint[(a,c)], P. Baud[(a)], N. Conil[(b)], P. Landrein[(b)]

[(a)] Institut de Physique du Globe de Strasbourg, 5 rue René Descartes, 67000, Strasbourg, France ; alexandra.rolland@unistra.fr ; patrick.baud@unistra.fr ; renaud.toussaint@unistra.fr

[(b)] Andra, Laboratoire de recherche souterrain de Meuse/Haute-Marne, RD 960, BP 9, 55290, Bure, France ; Nathalie.Conil@andra.fr; Philippe.Landrein@andra.fr

[(c)] Center for Advanced Study at the Norwegian Academy of Science and Letters, Oslo, Norway

*Corresponding author. Tel.: +33-3-68-85-00-87; E-mail address: arolland@unistra.fr; Postal address: EOST, 5 rue René Descartes, 67084, Strasbourg cedex, France

Abstract

We develop and test a methodology to infer paleostress from the morphology of stylolites within borehole cores. This non-destructive method is based on the analysis of the stylolite trace along the outer cylindrical surface of the cores. It relies on an automatic digitization of high-resolution photographs and on the spatial Fourier spectrum analysis of the stylolite traces. We test and show, on both synthetic and natural examples, that the information from this outer cylindrical surface is equivalent to the one obtained from the destructive planar sections traditionally used. The assessment of paleostress from the stylolite morphology analysis is made using a recent theoretical model, which links the morphological properties to the physical processes acting during stylolite evolution. This model shows that two scaling regimes are to be expected for the stylolite height power spectrum, separated by a cross-over length that depends on the magnitude of the paleostress during formation. We develop a non linear fit method to automatically extract the cross-over lengths from the digitized stylolite profiles. Results from cores obtained adjacent to the Andra Underground Research Laboratory located at Bure, France, show that different groups of sedimentary stylolites can be distinguished, and correspond to different estimated vertical paleostress values. For the Oxfordian formation, one group of stylolites indicate a paleostress of around 10 MPa, while another group yields 15 MPa. For the Dogger formation, two stylolites indicate a paleostress of around 10 MPa, while others appear to have stopped growing at paleostresses between 30 and 22 MPa, starting at an erosion phase that initiated in the late Cretaceous and continues today. The analysis of a tectonic stylolite from the Oxfordian formation indicates a major horizontal paleostress of between 14 and 20 MPa, which is in good agreement with the measured prevailing stress. Therefore, the method has a high potential for further applications on reservoirs or other geological contexts where stylolites are present.

Keywords: stylolite; paleostress; cross-over length; morphology analysis

Abbreviations:

- URL = Underground Research Laboratory

- COX = Callovo-Oxfordian

- FPS = Fourier power spectrum

- WPS = wavelet power spectrum

- RMS = root-mean-square

- MM = maximum-minimum height difference

- COR = correlation function

- RMS-COR = RMS correlation function

1. Introduction

Pressure-solution is a complex process that results in strain localization (localized dissolution) under particular stress conditions, and is at the origin of stylolite formation in several types of sedimentary rocks (e.g., carbonates ([1]-[5]), sandstones [6], and shales [7]). Stylolites have an undulated shape and are filled with organic matter, oxides, or clay particles. The latter has a significant role in the kinetics of the process ([8][9]). Stylolites are generally found to be more abundant with increasing depth and to initiate at mineralogical anomalies [10]. According to Fabricius and Borre [11], it is the burial stress that controls the pressure-solution process, while the temperature controls recrystallisation and cementation. Stylolites can be divided in several families, according to their orientation. Bedding-parallel stylolites are called sedimentary stylolites and differ from tectonic stylolites that form, in most cases, at a high angle to the bedding (i.e., sub-vertical). Sedimentary stylolites form due to lithostatic pressure, while tectonic stylolites form due to major compressive stresses related to the tectonic stress field (the Alps, the Pyrenees [33]), i.e., when the largest principal stress becomes horizontal rather than vertical. A few studies have tried to reproduce stylolites by simulating the pressure-solution process in the laboratory. However, such studies are inherently very difficult due to the slow kinetics of the process [7]. While some studies were based on loading aggregates in the presence of either saturated or non-saturated fluids ([9], [13][14]), others used an indenter to load crystals or surfaces, in the presence of fluid, whilst monitoring their evolution with time ([15], [16], [17], [18]). However, whilst one study produced microstylolites at the stressed contacts between grains [14], most experiments yielded other microstructural features, such as grooves ([19], [20], [21]). To our knowledge, stylolite growth has not yet been observed unambiguously in the laboratory. The study of the occurrence of stylolites, and their potential use as geological markers, therefore largely relies on the success of theoretical modelling. Numerical and analytical models have therefore been developed to study the growth of stylolites in presence of clay [1], or to reproduce the roughening from a preferential existing surface ([18], [22], [23]). More recently, Rolland et al. [24] proposed an analytical model that predicts the growth of a stylolite from a fluid-solid interface. This model gives a relation between the applied stress during the stylolite development and a characteristic length associated to the stylolite morphology. This relation was supported by numerical models studying the effect of disorder on the evolution of stylolite morphology ([24], [25]), and by some pilot studies on natural examples from various depths [26]. This approach therefore provides a tool to infer the stress history in various geological environments where stylolites are present.

Such an analysis hinges of course on a detailed description of the stylolite morphology, which to date has only been conducted in a few pilot studies ([27], [28]), on either 1D profiles or 2D surfaces. These analyses used digitized stylolite profiles or elevations, and were carried out on carbonate formations within newly-opened quarries or outcrops in the Cirque de Navacelles (Massif Central), Burgundy and Jura, Chartreuse, and Vercors mountains of France. In these studies, a characteristic length called the cross-over length (typically around the millimetre scale) was extracted by analysing the stylolitic profiles or surface height variations over different scales. The cross-over length separates the two scaling regimes predicted by the model [24]. On the small-scale, surface tension is the dominating process; while, on the large-scale, the roughness is driven by elastic interactions. In most of the geophysical/geological applied problems (such as reservoir/aquifer management, and nuclear waste repository management), the stress history of the sites is a fundamental issue. The systematic determination of the paleostress using stylolite morphology can therefore become an important tool in various applied contexts. This type of analysis demands core samples extracted *in-situ* from non-destructive boreholes (i.e., those were full core samples are retrieved) drilled over a representative depth interval within the target reservoir or aquifer. Obviously, these borehole samples need to contain stylolites. However, the use of cores from boreholes induces some geometrical limits linked, in particular, to their finite size and cylindrical shape. To our knowledge, only one example of such an analysis has been presented so far, on a core taken near from the Andra URL at Bure from the Dogger formation [29].

The objective of this study is to test the applicability of this method using a large number of stylolites within cores from borehole samples, and to develop a rigorous methodology to deduce the stress history of a reservoir using stylolite morphology. A previous study [30] showed the extensive presence of stylolites at various depths around the Andra URL at Bure. Therefore, this context is an excellent candidate to apply our methodology for the assessment of the paleostresses recorded by the stylolite morphology.

2. Geological context of the Bure URL

The Andra URL is located at Bure in the eastern part of the Paris Basin in France. Since 2001, it has been designed to study the feasibility of a nuclear waste repository in the COX claystones. The target horizon is surrounded by limestones from the Oxfordian and Dogger ages. Gunzburger [31] suggested that, from stress measurements and estimations around the Andra URL, the persistent deviatoric stress in the COX claystone formation (Fig. 1) is due to pressure-solution acting in the surrounding Oxfordian and Dogger limestone formations. This theory is supported by the presence of numerous stylolites within these limestone formations.

Boreholes were drilled adjacent to the Andra URL to study three horizons. However, from the 44 drilled boreholes, only 10 were non-destructive: 6 within the COX formation, 2 within the Oxfordian formation (EST204 and EST205), and 2 within the Dogger formation (EST433 and EST210). All of these 10 boreholes were drilled vertical (i.e., perpendicular to the surface and the bedding). The boreholes EST204 and EST205 were cored from the surface to depths of 508 and 510 m, respectively. Borehole EST433 was cored from 526 to 770 m, with punctual coring to 2001 m. Since the aim of this study is to sample stylolites over the largest depth interval possible, we selected the boreholes EST205 and EST433 as they present the highest potential in terms of available core. Furthermore, the analysis of sedimentary stylolites from these cores will be easier because the lithology is sub-horizontal.

The sampling of the stylolites within the cores could not be regular, since different zones were encountered within the borehole core samples: some presented regularly spaced stylolites (Fig. 2a), others presented damaged zones and multiple stylolites (Fig. 2b), and some zones present no stylolites (Fig. 2d). Additionally, stylolites that contained a fracture in their seam and slickolites (stylolites with tilted teeth) were not used in our study. Anastomosing stylolites (Fig. 2c) were frequent in the studied cores, but were not suitable for our purpose as they do not correspond to the strict hypothesis of the theoretical scenario. The above-mentioned stylolites were excluded from our dataset. A certain number of petrophysical measurements were recently performed on the cores studied here [32].

Our initial goal was to analyse already-opened stylolites and stylolites opened in the laboratory (Fig. 3). Roughness can be quantified precisely for these stylolites, at resolution down to a few tenths of micron using laser profilometry ([28], [33],[34], [35]). Obviously, this can only be done if enough open stylolites are available and/or if one can open enough stylolites. In the selected boreholes, as in the surrounding ones, open stylolites were scarce. Moreover, they often appear to have been weathered and hence affected by processes that could alter their morphology (Fig. 3a). Further, although it is sometimes possible to open a stylolite in the laboratory, significant fracturing usually occurs for stylolites that contain only a thin clay layer. In this instance, laser profilometry would scan a combination of the stylolite and the fracture. An example of this situation is given in Fig. 3b where a 4 cm x 2 cm sample broke partially along the stylolite and a fracture-like structure emerged. Therefore, to obtain the most-reliable results, we adopted a methodology that uses closed stylolites only (i.e., on 1D stylolitic profiles). To achieve our goal, a dedicated procedure was developed and will be outlined in section 4.

3. Theoretical background

To better understand how stylolite growth can be described, we will briefly review the model of Rolland et al. [24]. Using a simplified initial geometry (elongated fluid pocket enclosed between two contactless surfaces of infinite extent, Fig. 4), the manner in which the dissolution speed at the fluid-solid interface is affected by heterogeneities (by taking into account mechanical equilibrium and chemo-mechanical coupling) can be calculated. The surface is forming in a far-field stress tensor $\overline{\overline{\sigma^0}}$ where the horizontal principal components are isotropic ($\overline{\overline{\sigma^0_{xx}}} = \overline{\overline{\sigma^0_{yy}}}$) and smaller than the vertical principal component $\overline{\overline{\sigma^0_{zz}}}$. First, they show that the mechanical equilibrium at the solid-fluid interface is $\sigma.\hat{n} = -p\hat{n}$ where $p = -\sigma^0_{zz}$ is the fluid pressure. A local stress perturbation $\overline{\overline{\sigma^1}}$, induced by the irregularities of the surface, is combined to the far-field stress $\overline{\overline{\sigma^0}}$ and gives the stress field at the interface. They deduced the force perturbation due to the local stress perturbation $\overline{\overline{\sigma^1}}$ with $\delta f(x) = \sigma^1(x).\hat{n} = \sigma^0_s(\partial_x z)\hat{x}$. The chemo-mechanical coupling is expressed by the calculation of the dissolution speed normal to the solid-fluid interface as $v = m\Delta\mu$ where m is the mobility of the dissolving species depending on the dissolution rate k and molar volume Ω of the species at a given temperature, and $\Delta\mu$ is the chemical potential depending on the Helmoltz free energy, the change in normal stress, and on the curvature $\kappa = \partial_{xx}z$ of the interface. As for mechanical equilibrium, the velocity is affected by the perturbation of the surface giving a dissolution speed $v = v^0 + v^1$. Expressing the chemical potential as a function of the elastic free energy gives $u_e = \left[(1+\nu)\sigma_{ij}\sigma_{ij} - \nu\sigma_{kk}\sigma_{ll}\right]/4E$, where E is the Young's modulus and ν the Poisson's ratio. The dissolution speed is expressed as $v = -\partial_t z = m\Omega(\Delta u_e + \gamma\kappa)$ where γ is the surface tension. The calculation of the strain ϵ_{ij} and of the stress $\sigma_{ij} = \left[\epsilon_{ij} + \left(\nu\epsilon_{kk}\delta_{ij}/1-2\nu\right)\right]E/(1+\nu)$ using the Green function method (see details in [24]) permits the calculation of the stress perturbation σ^1 induced by the force perturbation $\delta f(x)$ and the elastic energy perturbation u^1_e. Combining all these equations yields an expression for the dissolution speed:

$$\partial_t z = \partial_{xx}z - \frac{l}{L_c}\int \frac{\partial_y z}{x-y}dy + \eta \qquad (1)$$

where η is a quenched noise due to the rock heterogeneities and $L_c = \gamma E / \beta P \sigma_s$ is a characteristic length where $\beta = [2\nu(1-2\nu)]/\pi$ is a dimensionless constant and P is the mean pressure. This equation describes the dominating process at both the small- and large-scale (i.e., at lengths inferior or superior to the characteristic length L_c). At the small-scale, i.e., $l \ll L_c$, surface tension is the dominating process and the model is reduced to $\partial_t z = \partial_{xx} z + \eta$.

At the large-scale, i.e., $l \gg L_c$, elastic interactions dominate and the model is reduced to $\partial_t z = -\frac{l}{L_c} \int \frac{\partial_y z}{x-y} dy + \eta$. Thus, this model highlights the occurrence of two regimes driven by two different processes. These two processes lead to two different scaling laws driven by $L^{(2H+1)/2}$ where H is the Hurst exponent which tends to 1 for the small-scale ([28], [36]) and to 0.5 for the large-scale [37]. Both regimes are separated by a characteristic length separating two scaling domains. This characteristic length appears in the morphology analysis and is called cross-over length.

4. Morphological analysis

As we have a large number of available stylolites in the cores, we developed a semi-automatic method to analyse our samples. The idea is to have a systematic procedure that can be applied when a lot of cores are available.

4.1. Procedure to digitize stylolites

The morphology analysis requires the extraction of a profile from the stylolite which has to be a single-valued function. The recipe for the digitization (the procedure is the same for slices or external profile) are listed below and illustrated in Fig. 5:

Step i: We took the core containing the stylolite and we placed it on a circular plateau that can rotate around a precisely fixed axis. We used a reflex camera with a large sensor (©NIKON D700) equipped with a 105 mm micro lens that allows us to have a high depth of field, and thus to have the curved surface in focus. We zoomed in to have the best resolution, which was 30 µm per pixel for our photographs (Fig. 5a). The sample was illuminated by two powerful spotlights on the front side to have the same illumination over the entire surface.

Step ii: To merge the pictures we used a standard graphics editing program (©Adobe Photoshop). We used grey level pictures (8-bits or 256 values) as we wanted to isolate the stylolite seam which appeared as black pixels. However, we had to clean the vicinity of the stylolite by removing some dark patches (Fig. 5b). Indeed, impurities or clay particles were often present in the rock and can be confused with the stylolite in the next step.

Step iii: We applied a threshold to isolate the black pixels constituting the stylolite seam from the surrounding rock (Fig. 5c). This threshold depended on the rock composition and shade. Indeed, all the cores did not have the same colour, the stylolites varied in thickness depending on the quantity of insoluble material, and heterogeneities were not always present in an equal quantity in each core. In our case, the threshold was set between 60 and 110 over 256 values. The sensitivity of this threshold was thoroughly tested (see Appendix 1).

Step iv: However, as mentioned in step ii, impurities can still be present and to remove them we applied another threshold on the size of the black pixels cluster (Fig. 5d). The smallest clusters, associated to the impurities, where then ignored.

Step v: As we need a single-valued function for the analysis, we interpolated the discontinued components (Fig. 5d, red segments). We chose a linear interpolation between these clusters.

Step vi: We extracted functions associated to the stylolite roughness (Fig. 5e). Three functions could be extracted: the top and bottom edges of the clusters, and the average line of the clusters. Our procedure to analyse the average line is presented in the next section.

4.2. Procedure to analyse the stylolite morphology

Stylolites show a self-affine geometry giving them the property to be invariant by affine transformation. For the horizontal variations Δx and Δy and the vertical variation Δz, the self-affinity can be defined as ([38], [39]): $\Delta x \rightarrow \lambda\Delta x$, $\Delta y \rightarrow \lambda\Delta y$ and $\Delta z \rightarrow \lambda^H\Delta z$. *H* is the Hurst exponent or roughness exponent which varies roughly between 0 and 1. Previous studies have analysed sedimentary stylolitic profile variations over different scales ([26], [28]). The results show two distinct scaling regimes, corresponding to different power laws. The exponent of these power laws is a function of the Hurst exponent *H*. Both regimes are separated by a characteristic length L_c, called cross-over length, typically within the millimetre scale. The small-scale regime shows a Hurst exponent around 1 and the large-scale regime has a Hurst exponent around 0.5.

To analyse the profiles, several signal processing methods exist. The main ones used to analyse stylolite or fracture morphologies are:

- the wavelet power spectrum – WPS – method ([29], [39], [40]) consisting of reconstructing the signal as a sum of different wavelets. It starts with a mother function which can be translated or dilated to find the corresponding form in the signal.
- the Fourier power spectrum – FPS – method ([29], [40]) consisting of analysing the wavelengths in the signal and reconstructing it as a sum of cosines and sinus.
- four other methods – RMS, MM, COR, RMS-COR – detailed in Candela et al. [40] and allows the analysis of stylolitic signals by analysing the height variations of the signal.

However, Candela et al. [40] ran tests on synthetic anisotropic self-affine surfaces to assess the reliance of each method. They found that the RMS-COR, the FPS, and the WPS techniques are the most reliable. In our case, if we look at their figure 4 in both directions, the error is minimum for the FPS method. Thus, we used the FPS technique to perform the spectral analysis of our stylolitic profiles. The spectrum was obtained by performing the calculation of the squared Fourier transform modulus $P[k]$ of the profile as a function of the wave-number k ($k = 2\pi/L$ where L is the wave-length).

Considering the self-affinity geometry of the stylolite, the FPS can be expressed as a function of the Hurst exponent, and by using the wave-length, yielding: $P[L] \approx L^{2H+1}$. If we plot the FPS as a function of L on a log-log graph, we have a very noisy spectrum (Fig. 6) with a lot of data at the small-scale and less and less data at the large-scale. To improve the analysis of the data, we resampled the data using logarithmic binning, giving a dot every 1.5 decade. This has the advantage to give a scale range of equal size in the logarithmic space.

To find the cross-over length we used an automatic least-square non-linear fit method as outlined in Ebner et al. [26]. It consists of fitting the resampled data in bilogarithmic space using the least-squares method. In this space, the model (two power laws with a cross-over to be determined) corresponds to a linear function over two parts with a cross-over function changing the scaling law from the small- to the large-scale. We look for a Hurst exponent around 0.5 ± 0.2 and 1 ± 0.2 for the large-scale and small-scale, respectively. Usually, to have a better measurement, more than an order of magnitude around the cross-over length is necessary. For a cross-over length around 1 millimetre, we need at least a 10 centimetre-sized sample. Then, the estimation of the cross-over length is iterative.

The uncertainties in Lc were determined using synthetic stylolite profiles. Following [41] and [42], we first created a white noise centred in 0 and bounded between -1 and 1. Then we created the wave-number $k_x = 2\pi/N$ where N is the length of the profile. Finally, we set the roughness of the stylolite and the cross-over length. In the spectral domain, we multiplied the white noise Fourier modes by the wave-number raised to a power depending on the Hurst exponent $L^{H+1/2}$. The discrimination between the small-scale and large-scale behaviours was achieved by setting the small-scale exponent so that the wave-number was larger than the one corresponding to the cross-over length, and vice versa. The synthetic stylolitic profile was finally obtained using an inverse Fourier transform. By running the analysis code several times on different synthetic stylolitic profiles, we were able to determine the error bars for the estimation of the cross-over length and of the Hurst exponents. The estimated error bars were 2.45% and 9.34% for small- and large-scale Hurst exponents, and 23.34% for the cross-over length. Fig. 6 shows the spectrum obtained from a synthetic profile. The repeatability of the method from the digitization to the spectral analysis was rigorously tested (see Appendix 2).

4.3. Data selection

We can extract two types of profile from the borehole core samples: planar profiles taken from a cut in the longitudinal direction of the core, and external profiles taken from the outer cylindrical surface of the core. Both types of data have pros and cons. For example, the slices require a long and destructive preparation process. On the other hand, the signal could be distorted by the curvature of the external profile. Since a non-destructive method is needed in a variety of applications, we examine the possible distortion associated with the curvature of the cylindrical profiles. Specifically, we investigated both synthetic and natural data, and compared the analysis of planar and cylindrical profiles to evaluate possible artefacts in the obtained cross-over lengths. We first analysed the external stylolitic profile (Fig. 7a), and four planar profiles, extracted from slices of a core from the Dogger horizon, taken a few centimetres apart (Fig. 7b).

The profiles were digitized using the procedure described above. We then plotted the FPS as a function of the length L on a bilogarithmic scale (Fig. 7c). Considering the error bars, the results show that the cross-over lengths are very close (except for profile 1). This small discrepancy can be explained by the fact that planar profiles are shorter than external profiles, and therefore the large-scale was less represented. The low resolution at the large-scale made the planar profiles analysis slightly more challenging. This issue was circumvented by making an average over several close planar profiles. Another difference lies in the periodic nature of the external profiles, contrarily to the planar ones. This periodicity certainly affects the determined Fourier amplitudes associated to the largest modes (around 1/4 of the perimeter or more), which should be excluded from the FPS analysis to provide a similar measure to the classical planar profiles.

To explore further these possible differences, the same analysis was performed on synthetic data. We created a synthetic stylolitic surface ([43], [44]), with known Hurst exponents (1 for the small-scale and 0.5 for the large-scale) and a cross-over length of 1 mm. Our analysis consisted of generating a white noise (here with values between -1 and 1 and centred in 0) on which we applied a fast Fourier transform – FFT. We imposed the Hurst exponents for the small- and large-scale in the frequency domain by a discrimination over k, the wave-number, such as for $k > k_c = 2\pi/L_c$, $H_s = 1$ for the small-scale and vice versa for large-scale with $H_l = 0.5$. We then came back to the spatial domain by performing a reversed FFT, and we obtained the synthetic stylolitic surface (Fig. 8a). The results (Fig. 8b) show that using the external profile, or the planar profile, gives non-distinguishable results, well within the error bars (they are closer to each other than the error bars of 23.34 % that correspond to the dispersion of the cross-over between independent planar profiles analysed in the same surface). We contend that this validates our non-destructive approach (i.e., we can characterise the morphology of stylolites using the external profiles of borehole core samples).

5. Results and discussion

We sampled stylolites from the Oxfordian and Dogger formation at depths ranging from 150 m to 320 m and from 650 to 750 m, respectively. 22 stylolites were selected from the Oxfordian formation, and 21 from the Dogger formation. Some of the stylolites displayed one scaling law, i.e., they could be described by a single Hurst exponent, lying typically between 0.6-0.8 (8 for Oxfordian limestones (Fig. 9a, 9b,) and 10 for Dogger limestones). Fig. 10 shows examples of stylolites that could be characterised by one scaling law. In many cases, these stylolites had a thick seam of insoluble materials that protruded from the surface of the core, likely due to soft material rearrangement along external profiles during the cutting. This influenced the small-scale by obscuring the fine details of the morphology. Alternatively, complex variations within the formation stress could also have produced one scaling law stylolites.

All the other stylolites show two scaling law regimes (16 and 11 for Oxfordian (Fig. 9e, 9f) and Dogger, respectively). Among the stylolites showing this behaviour, we observed some ill-defined spectrums, i.e., the fitted data for the small- (Fig. 9c) and large-scale (Fig. 9d) did not include enough data (less than one logarithmic order of magnitude). Moreover, some spectrums showed the possibility of a higher cross-over length (Fig. 11) in the large-scale but, in all cases, the right-part of the spectrums did not have enough data (3 or 4 points) to maintain the existence of a cross-over length. This was due to the geometrical limitation of our work on cores that have an inherently finite size. Therefore, we chose to exclude the cross-over lengths when the spectrums were ill-defined. Our results (Fig. 12a) provided cross-over length ranging from 0.45 mm to 4 mm for the Oxfordian stylolites, and from 0.8 mm to 6.2 mm for the Dogger stylolites. The normal distributions associated to the results are plotted in Fig. 12b and Fig. 12c for Oxfordian and Dogger, respectively. We observed no systematic variations of the cross-over length with depth. However, we can distinguish several groups of stylolites. For the Oxfordian stylolites, there are two groups: one with cross-over lengths around 1.2 mm, and one around 3 mm. The Dogger stylolites contained three distinct groups, characterised by the cross-over length: one around 1 mm, one around 2.3 mm, and one around 5 mm.

We calculated the corresponding paleostress using Equation (1) where $L_c = \gamma E/\beta P \sigma_s$. This equation can be simplified based on assumptions concerning the geological context. We applied the same simplification as [24] to the basin evolution:

- The major principal stress is vertical: σ_{zz}
- The horizontal principal stresses are isotropic: $\sigma_{xx} = \sigma_{yy}$
- The strain is uniaxial (i.e., we neglect horizontal elongation or shortening of the Paris Basin with respect to the vertical ones): $\sigma_{xx} = \sigma_{yy} = \frac{\nu}{1-\nu}\sigma_{zz}$

Using these assumptions, we have:

$$P = (2\sigma_{xx} + \sigma_{zz})/3 \qquad (2)$$

and,

$$\sigma_s = \sigma_{zz} - \sigma_{xx} \qquad (3)$$

And therefore, using Equation (1-3),

$$\sigma_{zz}^2 = \frac{\gamma E}{\alpha \beta L_c} \quad (4)$$

where α is a dimensionless geometrical factor depending on the Poisson's ratio ν ($\alpha = \frac{1}{3}\frac{(1+\nu)}{(1-\nu)}\frac{(1-2\nu)}{(1-\nu)}$). Using Equation (4), we assessed the paleostress σ_{zz} for sedimentary stylolites from the estimated cross-over length L_c. The results are presented on Fig. 13. For the calculation, we used $\gamma = 0.27$ J.m^{-2} which is the surface tension for a calcite-water interface [29]. X-ray diffraction measurements show a composition comprising of at least 97 % calcite. Hence, we used the Poisson's ratio of calcite $\nu = 0.32$ [45]. Considering the error induced by the cross-over length estimation, the calculated error on the paleostress was 11.67 %. Regarding the Young's modulus, as we can only measure the present value, we considered two hypotheses for the Young's modulus during stylolite formation: either the stylolite evolution stopped when the conditions for pressure-solution were not fulfilled anymore (closure of the pores and thus decrease of the dissolution process) or there was a significant change in the stress field. In the first scenario, we considered the Young's modulus to be different from the present value, i.e., correspond to the value rock at the end of the stylolitization process. In this case, we used a lower value of the Young's modulus for limestones $E = 15$ GPa [46]. In the second scenario, we considered the Young's modulus to be the same as the present value. In this case, we used values measured in the laboratory: between 23 to 36 GPa for the Oxfordian formation, and between 40 to 80 GPa for the Dogger formation. For the samples where no measure was done, we extrapolated the Young's modulus by taking a mean value between the nearest samples measured. These two scenarios resulted in the estimates of the paleostresses shown on the Fig. 13a and 13b. As a reference, we added two curves representing (i) the present lithostatic stress field ($\sigma_{zz} = \rho g z$ where $\rho = 2700$ kg.m^{-3} is the density, $g = 9.81$ m.s^{-2}, and z is the depth) and, (ii) the stress field at the maximum overburden that both limestone formations have seen. It was shown in a recent study [47] that the maximum erosion thickness that occurred during the late Cretaceous period is around 320 m. Regarding the samples from the borehole EST205, a thickness of 120 m has to be added to the overburden because of a localised erosion phase of the Barrois limestones.

Using the paleostress estimations of Fig. 13 we distinguished several groups at given stresses, corresponding to the groups observed previously in Fig. 12. In Fig. 13a the estimated stresses are equal or below the maximum stress that had affected the rocks. The Oxfordian formation shows two groups: one at a stress of around 10 MPa, and one around 15 MPa. The group of stylolites at 15 MPa appear to have been stopped in their evolution when the overburden was the highest. The Dogger formation shows three groups at 8, 11, and 17 MPa. All the corresponding stylolites indicate a stress lower than the prevailing stress, suggesting that, during their evolution, their formation was halted before a stress equal to the present-day stress was reached. However, if we consider the two groups close to the present vertical stress line, and if we convert the estimated stress at depth, a difficulty appears. Indeed, these rocks experienced a significant stress as they were buried to a depth of around 1000 m; therefore, it is not appropriate to consider a Young's modulus of 15 GPa for these rocks. Most of the data fall between the two references lines in Fig. 13b, indicating that stylolite evolution was stopped during the burial process at a stress higher than the current one or during the erosion phase in late Cretaceous.

In the Oxfordian formation, we still observe two groups: one around 12 MPa, and another one which shows a depth higher than the maximum overburden depth. The latter case is not valid since it is impossible for the rock to have been buried below the maximum overburden depth. In this case, the Young's modulus must be been too high and therefore a lower value must be considered for these stylolites. However, in the Dogger formation, we now only observe two groups. One of the three groups has now merged with another. Two stylolites indicate stresses of around 10 MPa, indicative of a halt in stylolite evolution at an early stage, at a stress inferior to the prevailing stress. The stylolites of the other group show a variation between the maximum overburden depth and the prevailing stress. In this case, the calculated stress is close to the present vertical stress. This suggests that (i) some stylolites are still active and, (ii) some stylolites progressively stopped growing at the beginning of the erosion phase.

To summarize, it seems that a low value of Young's modulus is more compatible with the Oxfordian formation, while the present Young's moduli are more appropriate for the Dogger formation. This leads to an average stresses of 10 and 15 MPa for the Oxfordian formation, and 10 and 30 to 22 MPa for the Dogger formation. In most cases, the stylolite evolution seems to have stopped at stresses between the maximum overburden stress and the present-day stress. This is corroborated by geochemical observations [30] showing two phases of stylolite reactivation in the late Cretaceous and the late Paleogene (beginning of the Alps formation). These observations suggest that stylolite evolution was halted during the erosion phase after the late Cretaceous.

As a pilot study we also analysed some of the tectonic stylolites within our borehole core samples. Locating a tectonic stylolite can be quite difficult as they are vertical or tilted, therefore the chance to have a non-destructive borehole crossing them are limited. We found three vertical tectonic stylolites in the vicinity of the depths 175 m, 215 m, and 260 m in the Oxfordian formation (borehole EST204). In all cases, the vertical stylolites crossed the sedimentary stylolites that were distributed every 10 cm (Fig. 14a). The vertical stylolite at 260 m crossed the core at the edge and shows displacements at each sedimentary stylolite in its path. For this reason, we cannot analyse a sufficiently long profile for that stylolite. The two other vertical stylolites cross the core longitudinally and in the middle. As for sedimentary stylolites, we digitized and analysed both of them. Only one, the stylolite at 215 m, showed a spectrum with the two-regime behaviour (Fig. 14b). The calculation of the associated horizontal paleostress (see argumentation for the first approximation in [33]) using the estimated cross-over length L_c = 1.89 mm and with the low Young's modulus E = 15 GPa and the measured Young's modulus E = 31 GPa, gives σ_H = 14.3 MPa and σ_H = 20.5 MPa, respectively. Considering the present stress field measurements ([48] and Fig.1), we see that the maximum horizontal principal stresses is σ_H = 14.5 MPa which shows a good agreement with our estimated value. As a tectonic stylolite form only under a specific stress field (such as for mountain formation), and since previous studies show numerous tectonic stages during Paleogene and Neogene periods (see for example André et al. [30]), we suggest that this tectonic stylolite initiated during one of these periods, and stopped when the major principal horizontal stress changed orientation.

6. Conclusion

In this paper, we developed a rigorous methodology to infer paleostresses from core samples taken from boreholes. Our procedure is based on a recent model [32] which relates the paleostresses to the morphology of stylolites. Using high-resolution photographs of stylolites, profiles were digitized and analysed by calculating the Fourier power spectrum. The resulting characteristic length, called the cross-over length, was used to estimate the associated paleostress. Numerous difficulties arose from the use of borehole core samples, such as geometrical constraints linked to their finite size. We show, on both natural and synthetic examples, that the morphology analysis performed on cylindrical contours and planar profiles yield comparable results. It is therefore possible to use the cylindrical contour to infer the paleostresses using a non-destructive procedure. We applied our new methodology to analyse a large number of stylolites in limestone formations surrounding the Andra URL at Bure (eastern Paris Basin, France). The paleostresses deduced from sedimentary stylolites are compatible with recent data on the evolution of the Paris basin. Pilot work on a tectonic stylolite also results in a consistent estimation with respect to the present stress conditions. However, we were limited by the small number of tectonic stylolites found in the studied boreholes. More work is needed on a larger number of tectonic stylolites in the studied area. Our analysis suggests that the paleostress determination in various geological environments can be better determined when both horizontal and vertical non-destructive boreholes are available.

Acknowledgments

The authors want to thank Thierry Reuschlé, Bertrand Renaudie, Jean-Daniel Bernard, Alain Steyer and Yves Bernabé for technical support and fruitful discussions. This work is funded by Andra.

Appendices

A1. Sensitivity to the threshold in the digitization procedure

To test the sensitivity to the thresholds in the digitization procedure we selected a segment of a stylolite from the Dogger formation (borehole EST433) from core EST44535 taken at a depth of 719.56 m. We used various thresholds on the grey levels (40, 60 and 80) and two different thresholds on the cluster size (800 and 1000). That stylolite was analysed with a threshold on grey levels of 60 and a threshold on the cluster size of 1000 (arbitrary threshold depending on the continuity of the seam or on the size of heterogeneities present in the host rock) and the cross-over length was found to be 0.78 mm. In the following, we will mention the different cases for the thresholds as [grey level threshold - cluster size threshold]. After the digitization we extracted the corresponding functions and we analysed them as described in section 4.2. Fig. A1a shows the results for the analyses with a threshold on the grey levels of 40. The seam of the stylolite is not well defined and thus the morphology is biased. We could not extract from the FPS the two-regimes behaviour. Fig. A1b and A1c show the results for the thresholds on the grey levels of 60 and 80. In the case of the threshold [60 - 800], we observe a two-regimes behaviour but the cross-over length is lower than what we expect and the Hurst exponent for large scales is a bit high. However, the thresholds [60 - 1000], [80 - 800] and [80 - 1000] show Hurst exponents and cross-over lengths close to what we expect. Therefore, if we under estimate the thresholds, the morphology is more affected than if we over estimate them. It is important to have a good definition of the seam to avoid to affect the morphology. An over estimation of the thresholds induces more noise in the data but it is mixed up with the existing noise and it is therefore preferable than a lack in the data induced by an under estimation.

A2. Repeatability of the method

We tested the repeatability of the method by doing the analysis several times on the same stylolite. We repeated the whole procedure from the digitization to the FFT analysis. Regarding the digitization, Fig. A2a shows the extracted function from the first analysis in blue and from the second analysis several months later in red. We see that they are almost identical. To assess the differences between both traces we calculated the absolute difference between both traces (Fig. A2b). The maximum difference corresponds to 18.3 % of the total amplitude of the stylolite while the mean of the difference corresponds to less than 1 % of the amplitude. Regarding the analyses results, Fig. A2c shows the spectrum of the first analysis and Fig. A2d shows the spectrum obtained after the second analysis. We see that the Hurst exponents are almost the same and that the cross-over lengths have a difference of 24.8 % which is close to the error bar.

References

[1] Bathurst R.G.C. Carbonate sediments and their diagenesis. Amsterdam/London/New York: Elsevier;1971.

[2] Park W.C. and E.H. Schot. Stylolites: their nature and origin. J Sediment Petrol 1968; 38: 175-91.

[3] Stockdale P.B. Stylolites: their nature and origin. Indiana University Studies 1922; 9: 1-97.

[4] Stockdale P.B. Rare stylolites. American J Sci 1936; 32: 129-33.

[5] Stockdale P.B. Stylolites: primary or secondary? J Sediment Petrol 1943; 13: 3-12.

[6] Heald M.T. Stylolites in sandstones. J Geol 1955; 63: 101-14.

[7] Rutter E.H. Pressure solution in nature, theory and experiment. J Geol Soc 1983; 140: 725-40.

[8] Aharonov E. and R. Katsman. Interaction between pressure solution and clays in stylolite development: insights from modelling. American J Sci 2009; 309:607-32.

[9] Renard F., P. Ortoleva and J.P. Gratier. Pressure solution in sandstones: influence of clays and dependence on temperature and stress. Tectonophysics 1997; 280: 257-66.

[10] Lind I.L. Stylolites in chalk from leg 130, Ontong Java Plateau. Proc ODP Sci Results 1993; 130: 673-86.

[11] Fabricius I.L. and M.K. Borre. Stylolites, porosity, depositional texture and silicates in chalk facies sediments. Ontong Java Plateau – Gorm and Tyra fields, North Sea. Sedimentology 2007; 54: 183-205.

[12] Renard F., D. Dysthe, J. Feder, K. Bjørlykke and B. Jamveit. Enhanced pressure solution creep rates induced by clay particles: experimental evidence in salt aggregate. Geophys Res Lett 2001; 28: 1295-8.

[13] Cox S.F. and M.S. Paterson. Experimental dissolution-precipitation creep in quartz aggregates at high temperatures. Geoph Res Lett 1991; 18:1401-04.

[14] Gratier J.P., L. Muquet, R. Hassani and F. Renard. Experimental microstylolites in quartz and modelled application to natural stylolitic structures. J Struct Geol 2005; 27: 89-100.

[15] Gratier J.P. Experimental pressure solution of halite by an indenter technique. Geoph Res Lett 1993; 20: 1647-50.

[16] Gratier J.P., L. Jenatton, D. Tisserand and R. Guiguet. Indenter studies of the swelling, creep and pressure solution of Bure argillite. App Clay Sci 2004; 26; 459-72.

[17] Karcz Z., E. Aharonov, D. Ertas, R. Polizzotti and C.H. Scholz. Deformation by dissolution and plastic flow of a single crystal sodium chloride indenter: an experimental study under the confocal microscope. J Geoph Res 2008; 113: B04205.

[18] Laronne Ben-Itzhak L., E. Aharonov, R. Toussaint and A. Sagy. Upper bound on stylolite roughness as indicator for the duration and amount of dissolution. Earth and Planet Sci Let 2012; accepted.

[19] Den Brok S.W.J. and J. Morel. The effect of elastic strain on the microstructure of free surfaces of stressed minerals in contact with an aqueous solution. Geoph Res Lett 2001; 28: 603-06.

[20] Dysthe D., F. Renard, J. Feder, B. Jamtveit, P. Meakin and T. Jøssang. High resolution measurements of pressure solution creep. Phys Rev E 2003; 68: 011603.

[21] Koehn D., J. Arnold, B. Jamtveit and A. Malthe-Sørenssen. Instabilities in stress corrosion and the transition to brittle failure. American J Sci 2003; 303: 956-71.

[22] Koehn D., F. Renard, R. Toussaint and C.W. Passchier. Growth of stylolite teeth patterns depending on normal stress and finite compaction. Earth and Planet Sci Lett 2007; 257: 582-95.

[23] Ebner M., D. Koehn, R. Toussaint and F. Renard. The influence of rock heterogeneity on the scaling properties of simulated and natural stylolites. J struct Geol 2009; 31:72-82.

[24] Rolland A., R. Toussaint, P. Baud, J. Schmittbuhl, N. Conil, D. Koehn et al. Modeling the growth of stylolites in sedimentary rocks. J Geoph Res 2012; 117: B06403.

[25] Koehn D., M. Ebner, F. Renard, R. Toussaint and C.W. Passchier. Modelling of stylolite geometries and stress scaling. Earth and Planet Sci Let, Accepted.

[26] Ebner M., D. Koehn, R. Toussaint, F. Renard and J. Schmittbuhl. Stress sensitivity of stylolite morphology. Earth and Planet Sci Lett 2009; 277: 394-98.
[27] Brouste A., F. Renard, J.P. Gratier and J. Schmittbuhl. Variety of stylolites' morphologies and statistical characterization of the amount of heterogeneities in the rock. J Struct Geol 2007; 29: 422-34.
[28] Schmittbuhl J., F. Renard, J.P. Gratier and R. Toussaint. Roughness of stylolites: implications of 3D high resolution topography measurements. Phys Rev Lett 2004; 93: 238501.
[29] Renard F., J. Schmittbuhl, J.P. Gratier, P. Meakin and E. Merino. Three-dimensional roughness of stylolites in limestones. J Geophys Res 2004; 109: B03209.
[30] André G., C. Hibsch, S. Fourcade, M. Cathelineau and S. Buschaert. Chronology of fracture sealing under a meteoric fluid environment: Microtectonic and isotopic evidence of major Cainozoic events in the eastern Paris Basin (France). Tectonophysics 2010; 490:214-28.
[31] Gunzburger Y. Stress state interpretation in light of pressure-solution creep: numerical modelling of limestone in the Eastern Paris Basin, France. Tectonophysics 2010; 483: 377-89.
[32] Rolland A. Andra technical documentation 2011. DRPAMFS120004.
[33] Ebner M., R. Toussaint, J. Schmittbuhl, D. Koehn and P. Bons. Anisotropic scaling of tectonic stylolites: A fossilized signature of the stress field? J Geophys Res 2010; 115: B06403.
[34] Neuville A., R. Toussaint, J. Schmittbuhl, D. Koehn and J.-O. Schwarz. Characterization of major discontinuities from borehole cores of the black consolidated marl formation of Draix (French Alps). Hydro Proc 2011; 186: 1064.
[35] Laronne Ben-Itzhak L., E. Aharonov, R. Toussaint and S. Amir. Upper bound on stylolite roughness as indicator for amount of dissolution. Earth and Planet Sci Let, Accepted.
[36] Roux S. and A. Hansen. Interface roughening and pinning. J Phys I 1994; 4: 515-38.
[37] Tanguy A., M. Gounelle and S. Roux. From individual to collective pinning: Effect of long-range elastic interactions. Phys Rev E 1998; 58: 1577-90.
[38] Barabási A. and H. Stanley. Fractal concepts in surface growth. Cambridge University Press; 1995.

[39] Simonsen I., A. Hansen and O.M. Nes. Determination of the Hurst exponent by use of wavelet transforms. Phys Rev E 1998; 58: 2779-87.

[40] Candela T., F. Renard, M. Bouchon, A. Brouste, D. Marsan, J. Schmittbuhl et al. Characterization of fault roughness at various scales: implications of three-dimensional high resolution topography measurements. Pure and Applied Geoph 2009; 166:1817-51.

[41] Press W.H., S.A. Teukolsky, W.T. Vetterling and B.P. Flannery. Numerical Recipes. New York: Cambridge Univ Press; 1992.

[42] Neuville A., R. Toussaint and J. Schmittbuhl. Hydrothermal coupling in a self-affine rough fracture. Phys Rev E 2010; 82: 036317.

[43] Méheust Y. and J. Schmittbuhl. Geometrical heterogeneities and permeability anisotropy of rough fractures. J Geoph Res 2001; 106: 2089-102.

[44] Méheust Y. and J. Schmittbuhl. Scale effects related to flow in rough fractures. Pure and Applied Geoph 2003; 160: 1023-50.

[45] Mavko G., T. Mukerji and J. Dvorkin. The Rock Physics handbook. Cambridge University Press 1998.

[46] Clark, S.P.J. Handbook of physical constants. Geological Society of New-York 1966.

[47] Blaise T., M. Cathelineau, M.C. Boiron and N. Clauer. Extensive mineral authigenesis in Triassic sandstones from eastern Paris Basin: which thermal and fluid history? Accepted in Physics and Chemistry of the Earth.

[48] Wileveau Y., F.H. Cornet, J. Desroches and P. Blumling. Complete in situ stress determination in an argillite sedimentary formation. Phys Chem of the Earth 2007; 32: 866-78.

Figure captions

Figure 1: Estimated stress profiles at the URL based on in-situ stress measurements (modified from Wileveau et al. [48]). Gunzburger [31] suggests that the persistent deviatoric stress in the Callovo-Oxfordian claystone formation is due to slow processes in the surrounding limestone formations as pressure-solution.

Figure 2: Photographs of the studied material. a) Core from the EST433 borehole (712.55 to 713.60 m) with several distinct stylolites. The left image is a zoom of the red box. b) Core from the EST433 borehole (718.69 to 719.75 m) with a zone of multiple stylolites and damaged parts. The left image is a zoom of the red box. c) Core from the EST433 borehole (719 m) with anastomosing stylolites. d) Core from the EST433 borehole (699.70 to 700.86 m) with no stylolites along 1 m.

Figure 3: The issue of open and opened stylolites. a) Open stylolite taken from the borehole EST433 at 719 m deep with weathered surface. b) Oxfordian limestone sample (4 cm*2 cm) opened in the laboratory. We observe a combination of fracture-like structure (#1, light colour corresponding to the surrounding rock) and of stylolite-like structure (#2, dark colour corresponding to the insoluble matters in the stylolitic seam). We observe similar features on the sample coming from the borehole EST433.

Figure 4: Geometry of the solid-fluid interface modified from Rolland et al. [32].

Figure 5: Main steps to digitize stylolites. a) Step i - Take pictures with high resolution. b) Step ii - Merge and clean pictures. c) Step iii - Isolate the stylolite – First threshold on the grey-level. d) Step iv and v - Isolate the stylolite – Second threshold on the cluster size and interpolate the discontinue parts. e) Step vi - Extract the functions associated with the stylolite. Axes are in pixels.

Figure 6: Spectrum obtained after analysis of a synthetic stylolitic profile. The Fourier power spectrum is represented as a function of the wave-length. The noisy continuous line represents the raw spectrum

obtained after the analysis. The discontinuous line with open circles represents the logarithmic binning, the data being resampled every each 1.5 tenth of order. The continuous line with filled circles corresponds to the modeled data. The cross is the estimated cross-over length calculated by the code. The estimated Hurst exponents for small and large scale (*Hs* and *Hl* respectively) are in the up-left corner.

Figure 7: Comparison of the planar and external profiles spectrums. a) We analysed the external stylolitic profile from the 10 cm diameter core taken from the borehole EST433 at 720 m deep. b) The core was cut into 3 slices allowing the analysis of 4 planar profiles extracted from each side of the slices. c) Result of the FPS analysis. The Fourier power spectrum is represented as a function of the wave-length. The spectrum and cross-over lengths obtained are very similar.

Figure 8: Test analyses on a synthetic stylolitic surface. a) Synthetic stylolitic surface. The black surface cutting along the diameter simulates a planar profile. The blue surface cutting along a perimeter simulates an external contour of a core. b) Results of the test analyses for the planar profile and the external contour. The Fourier power spectrum is represented as a function of the wave-length.

Figure 9: Representative examples of spectrums resulting from the analyses of stylolites in Oxfordian limestones. The Fourier power spectrum is represented as a function of the wave-length. Samples a) from core EST43772 at 175.80 m and b) from core EST43790 at 231.40 m show a behaviour with one scaling law described by one Hurst exponent H in red. Samples c) from core EST06683 at 158.73 m and d) from core EST06683 at 159.23 m show the two regimes behaviour. However, these samples were disregarded due to the poor quality of the fit. Samples e) from core EST43792 at 253.92 m and f) from core EST06945 at 313.36 show the two-regimes behaviour and are typical of the ones used to infer the paleostresses.

Figure 10: Details of the stylolites showing a one scaling law behaviour. a) Core EST43772 at 175.80 m and b) core EST43790 at 231.40 m.

Figure 11: Examples of spectrum suggesting a higher cross-over length (>10 mm). a) Core EST43798 at 259.18 m. The spectrum shows a change in the slope around 16 mm. b) Core EST44522 at 739.61 m. The spectrum shows a change in the slope around 20 mm.

Figure 12: Summary of the estimated cross-over lengths. a) Cross-over length as a function of the sample depth for the stylolites from the Oxfordian and Dogger formations. The error bars represent 23.34% of the value. b) Normal distribution of the resulting cross-over lengths for the Oxfordian limestones. c) Normal distribution of the resulting cross-over lengths for the Dogger limestones. Some of the extreme values were excluded because of ill-defined spectrums.

Figure 13: Results of the paleostress calculation for the Oxfordian and Dogger formations. The error bar on the data is 11.67%. a) The lower bound of the paleostress is calculated using Young's modulus equal to the lower limit for carbonates i.e. 15 GPa. b) The upper bound is calculated using the Young's modulus measured in the laboratory on selected samples. For reference, we plotted on both graphs a line corresponding to the current lithostatic stress (i) and a line corresponding to the maximum overburden for both formations (ii - around 440 m of eroded ground for the borehole EST205 and 320 m for the borehole EST433) according to recent estimations [47].

Figure 14: Tectonic stylolite analysis. a) Detail of the selected tectonic stylolite (core EST32219 in the vicinity of 215.2 m). The horizontal seam is the tectonic stylolite crossed by a sedimentary stylolite (vertical seam). b) Spectrum resulting of the analysis showing the two-regime behaviour.

Figure A1: Sensitivity test of the procedure. Both value of thresholds are tested, the value on the grey levels and on the cluster size. a) Resampled spectrum data for threshold values of[40 - 800] and [40 - 1000]. The stylolite seams are framed with the corresponding colour. b) Modeled data and cross-over lengths for threshold values of [60 - 800] and [60 - 1000]. The stylolite seams are framed with the corresponding colour. c) Modeled data and cross-over lengths for threshold values of [80 - 800] and [80 - 1000]. The stylolite seams are framed with the corresponding colour.

Figure A2: Repeatability analysis of the method performed by analysing twice the same stylolite. a) Profiles of the first (blue) and the second (red) analysis performed independently. They are almost identical. b) Differences between both traces. The mean difference represents less than 1 % of the total amplitude of the stylolite. Spectrums resulting from c) the first analysis and d) the second analysis. The Hurst exponents are almost the same while the cross-over lengths difference is in the error bar of the method.

Figure
Click here to download high resolution image

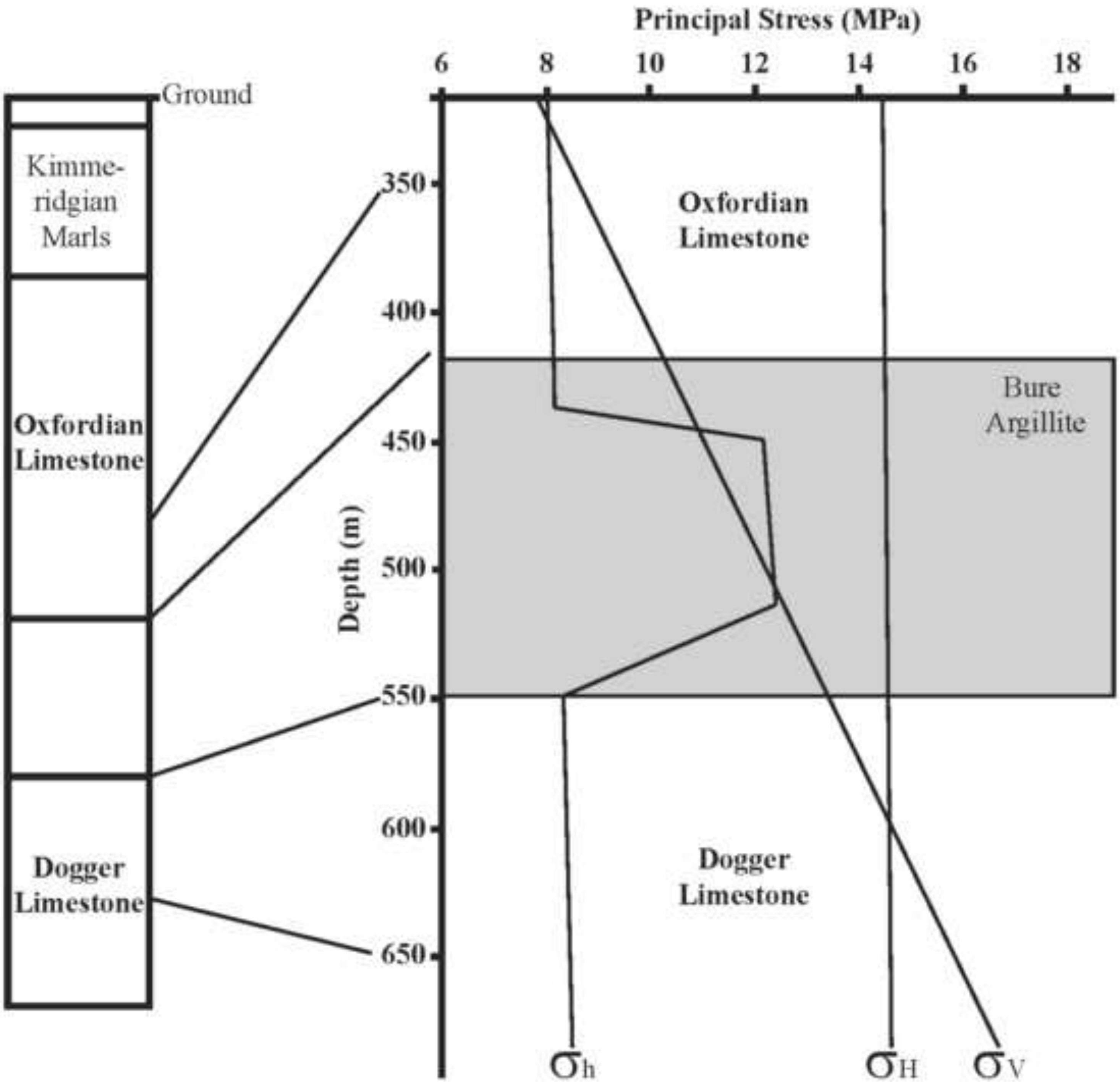

Figure
Click here to download high resolution image

Figure

Click here to download high resolution image

Figure
Click here to download high resolution image

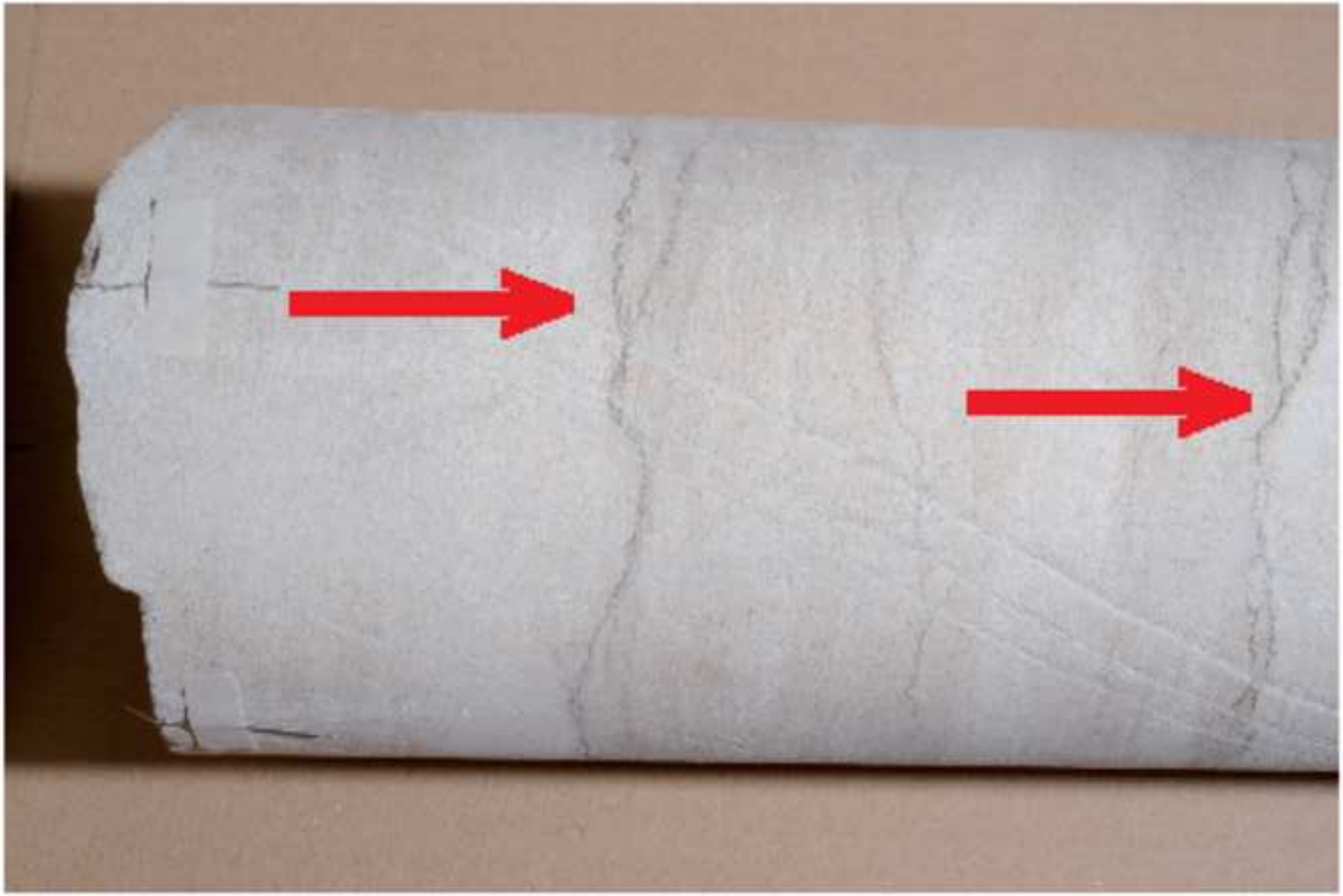

Figure
Click here to download high resolution image

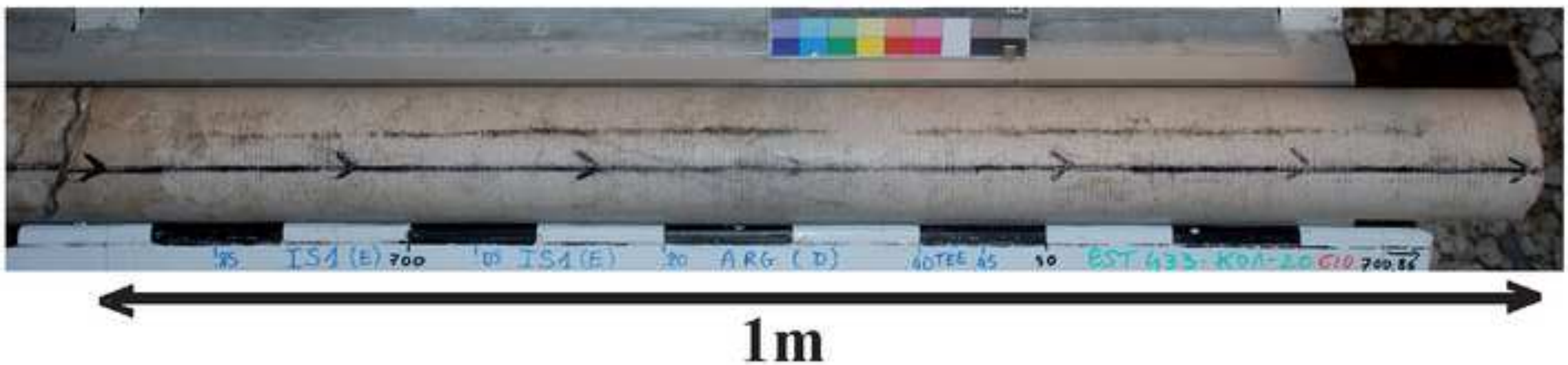

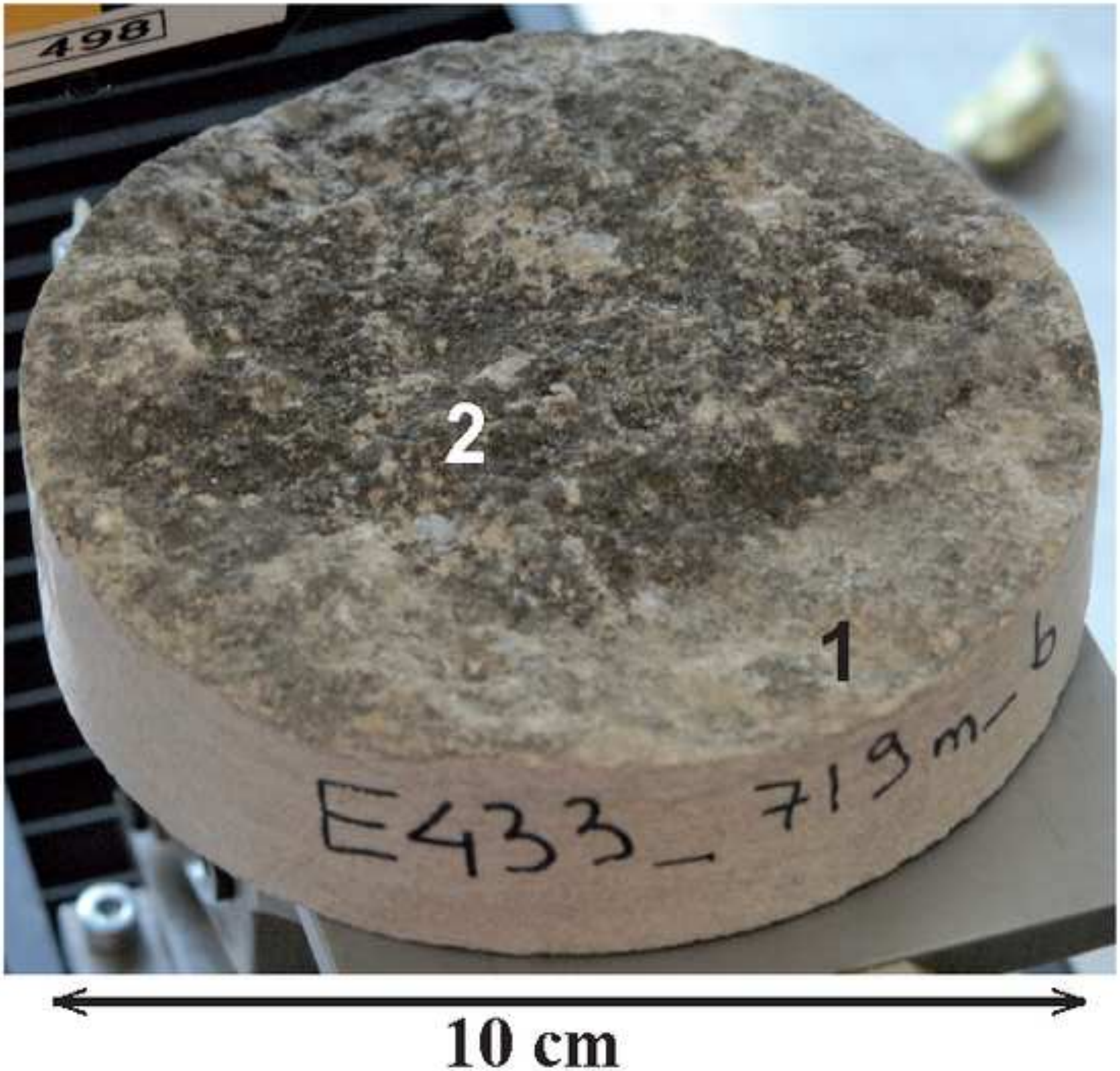
498
2
1
E433_ 719m_ b
10 cm

Figure
Click here to download high resolution image

Figure
Click here to download high resolution image

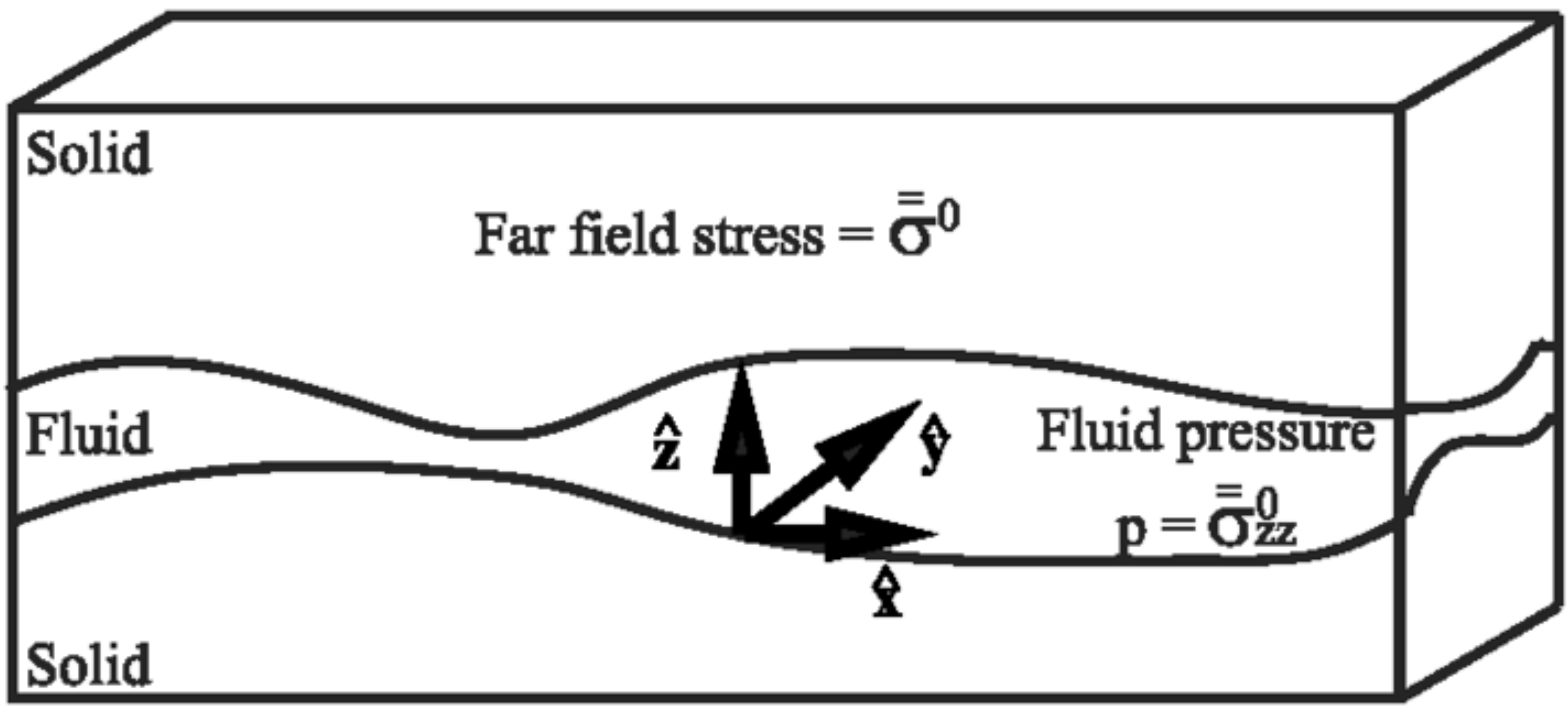

Figure
Click here to download high resolution image

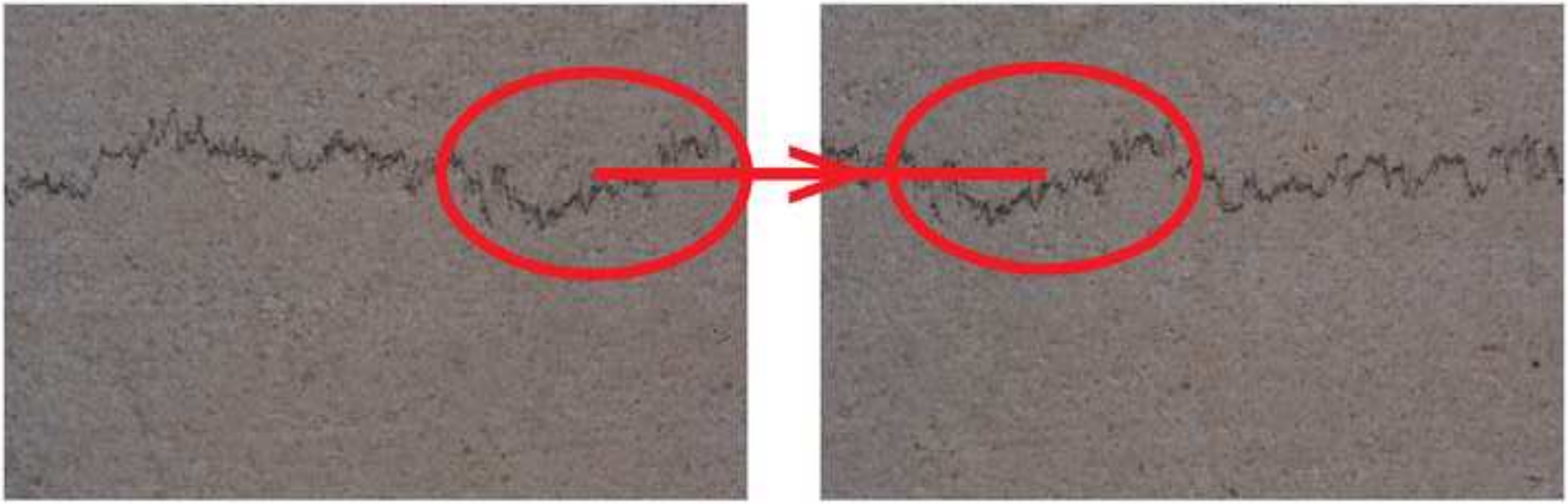

Figure
Click here to download high resolution image

Figure
Click here to download high resolution image

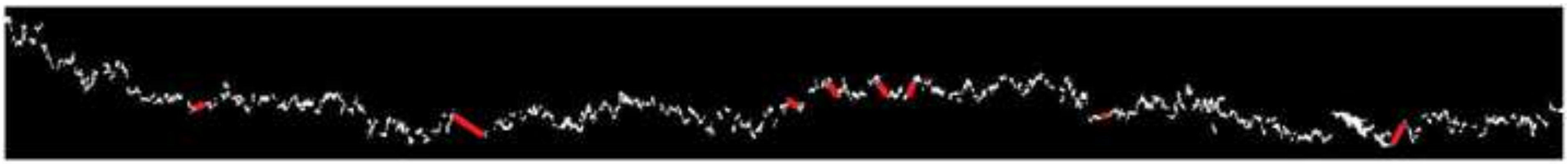

Figure
Click here to download high resolution image

Figure
Click here to download high resolution image

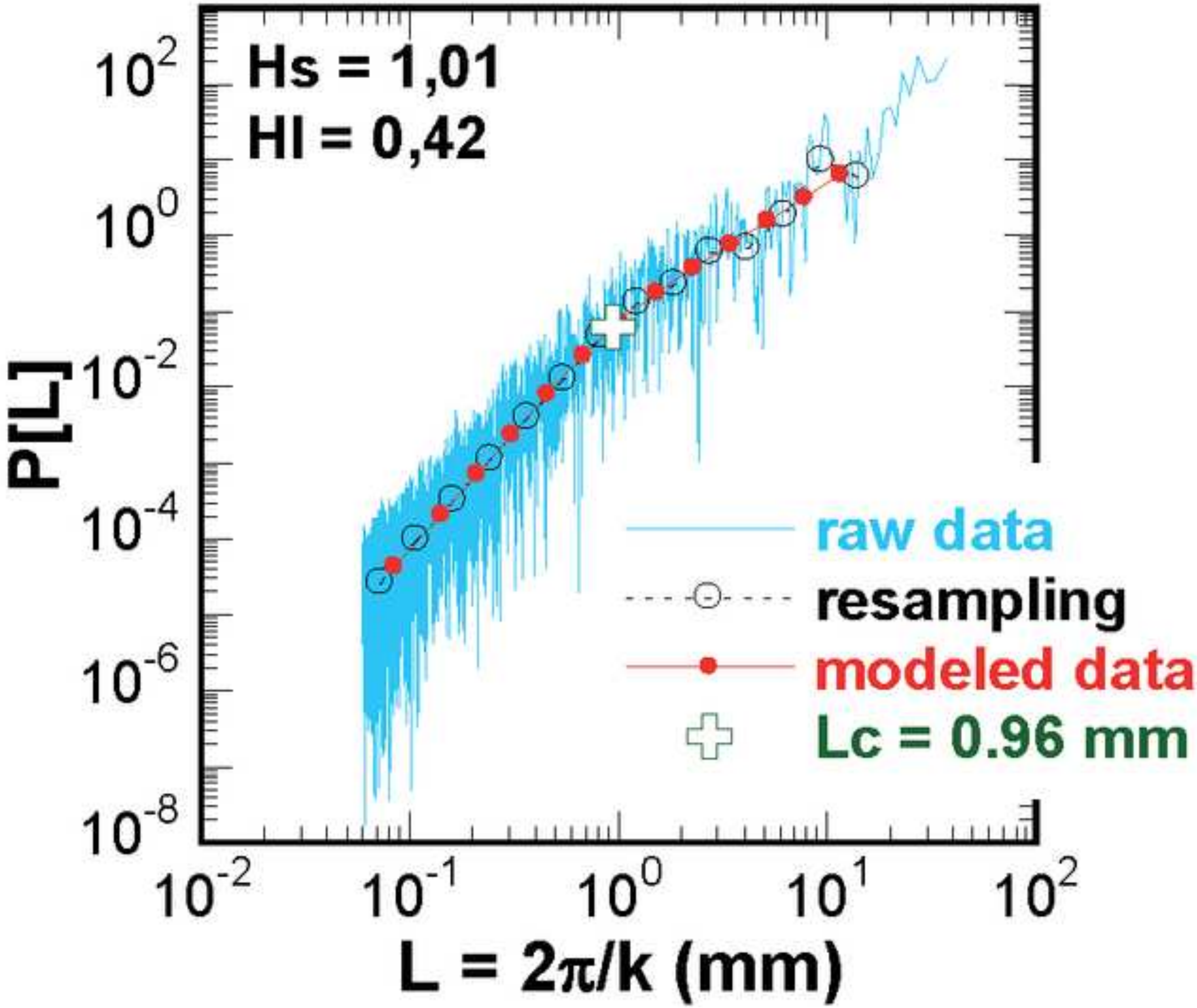

Figure
Click here to download high resolution image

Figure
Click here to download high resolution image

Figure
Click here to download high resolution image

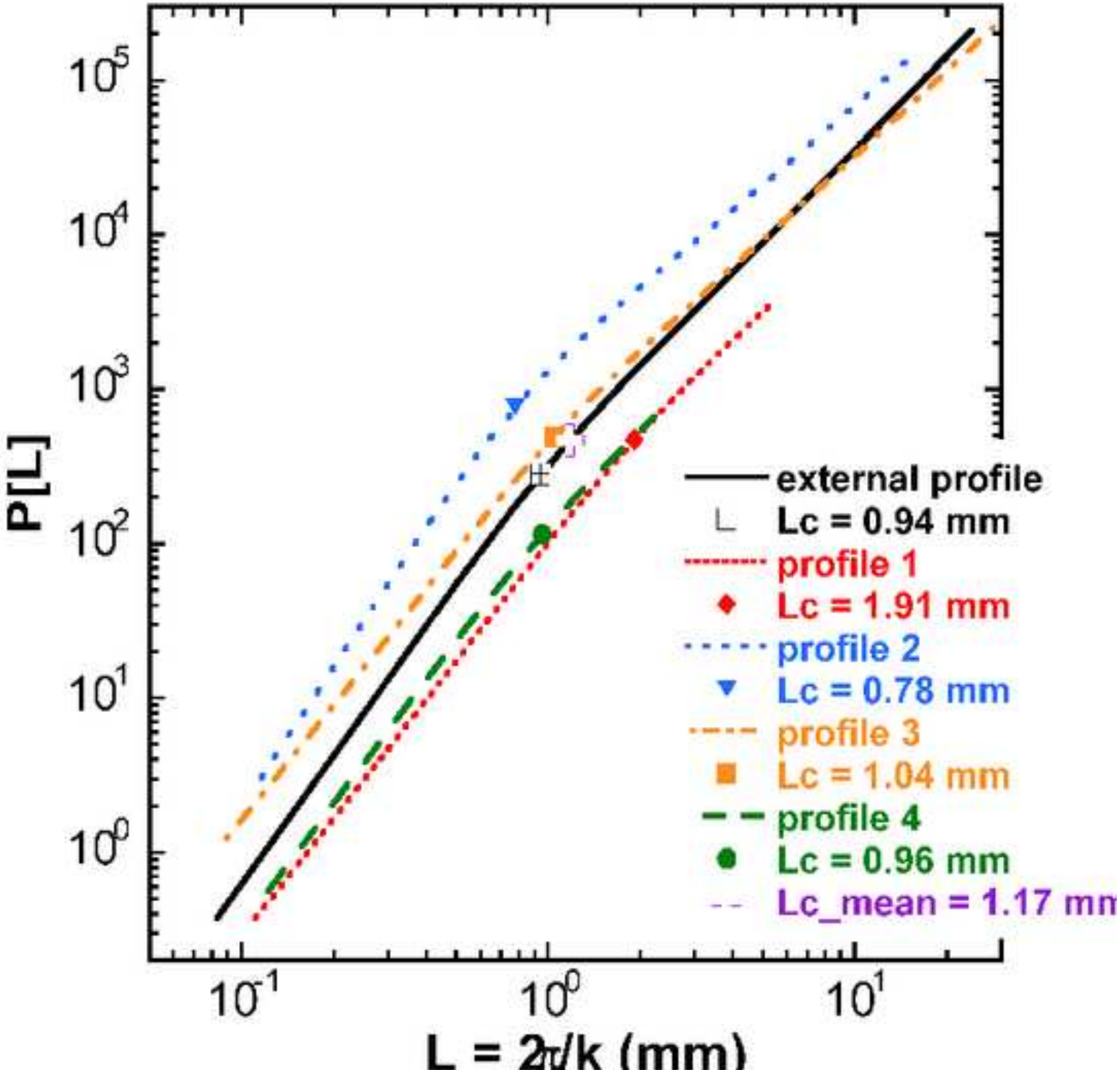

Figure
Click here to download high resolution image

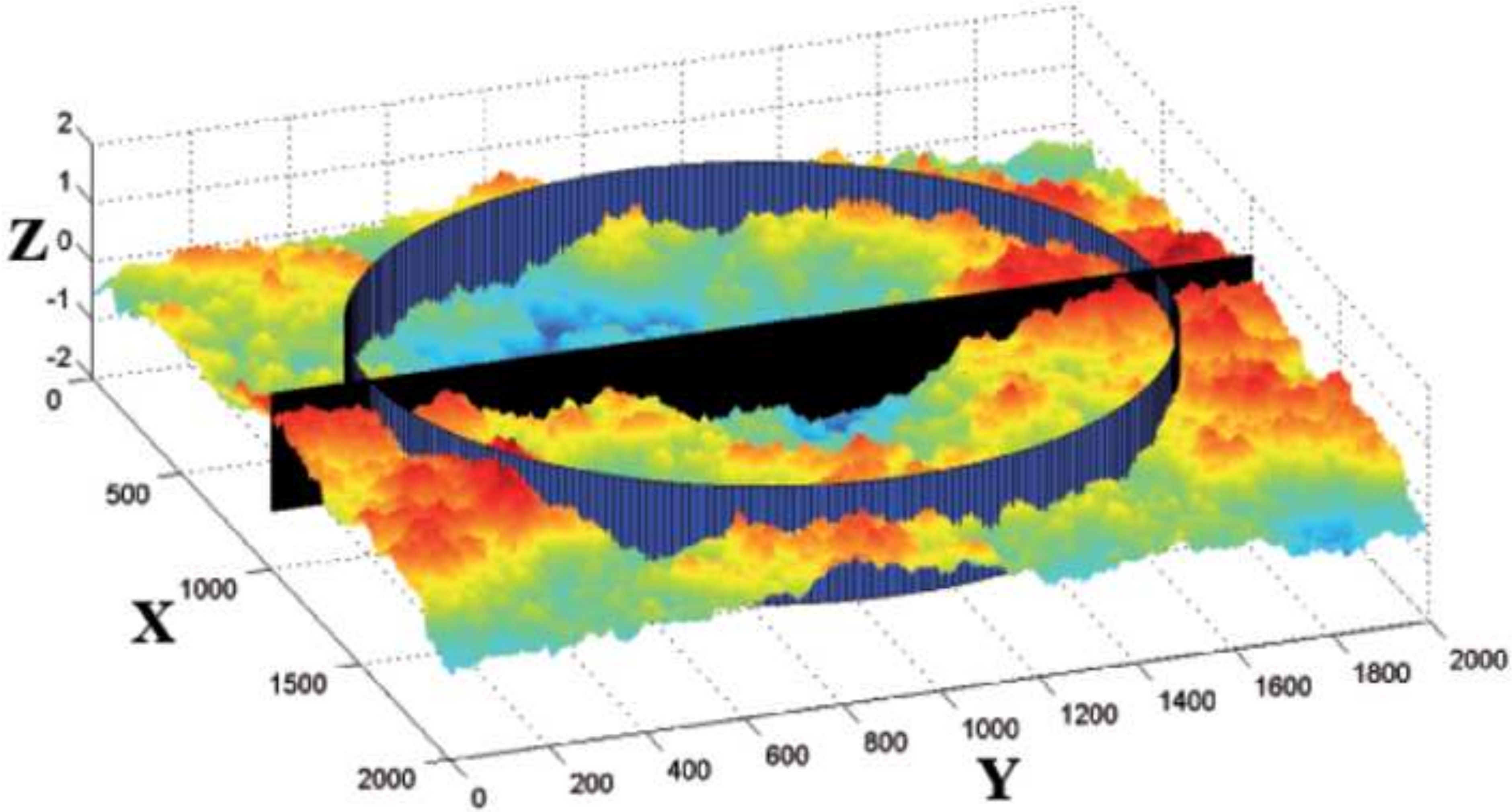

Figure
Click here to download high resolution image

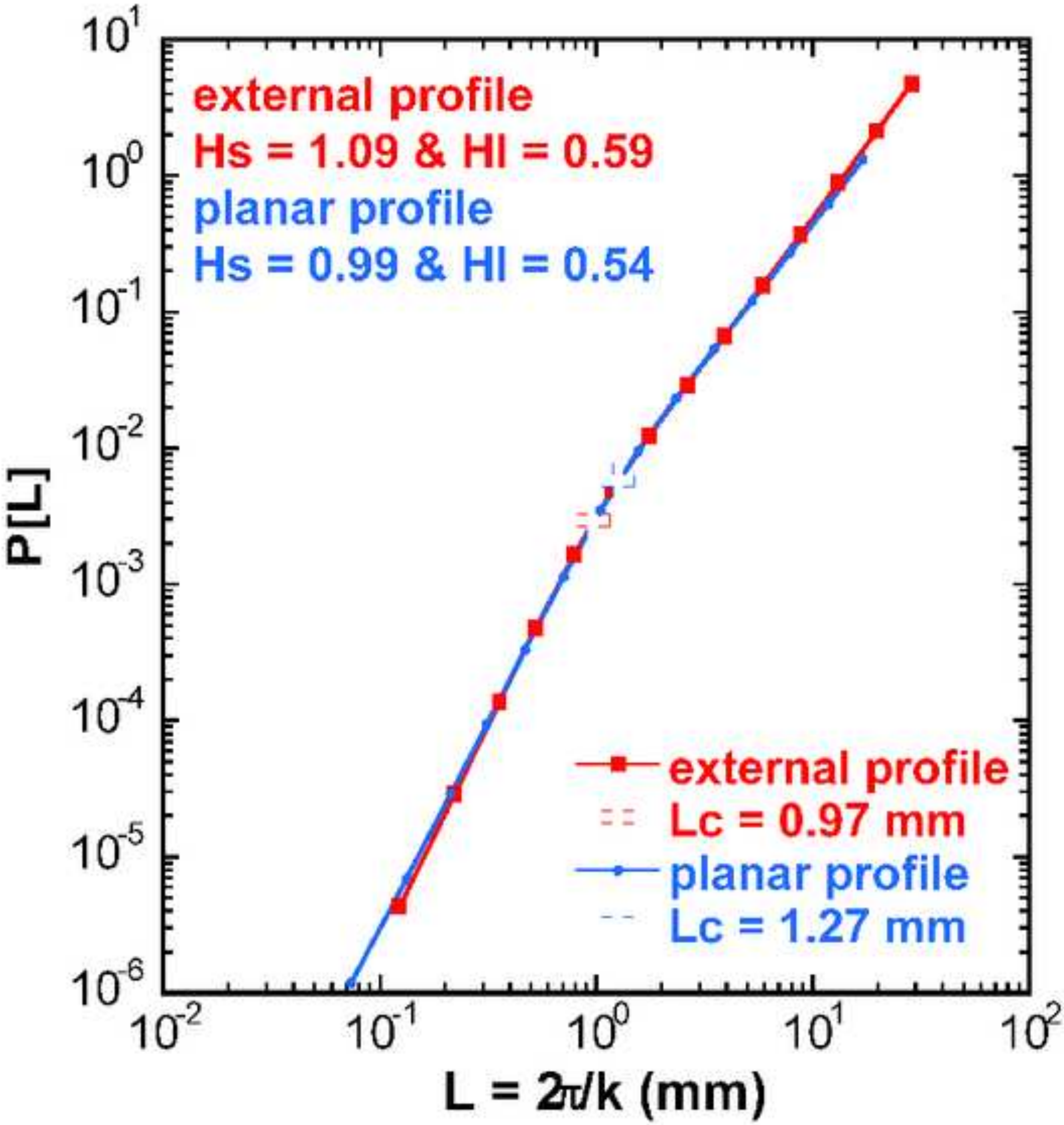

Figure
Click here to download high resolution image

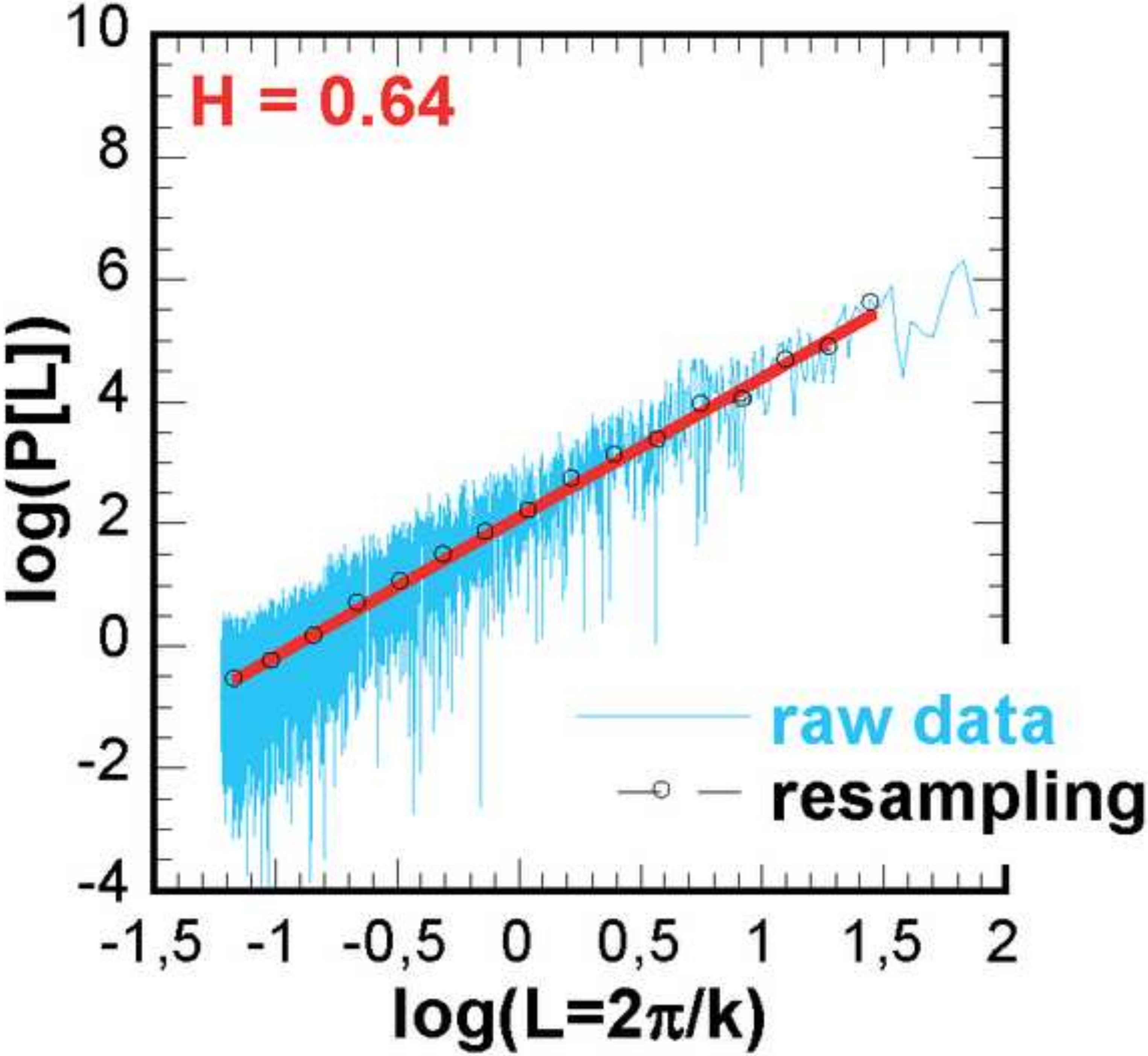

Figure
Click here to download high resolution image

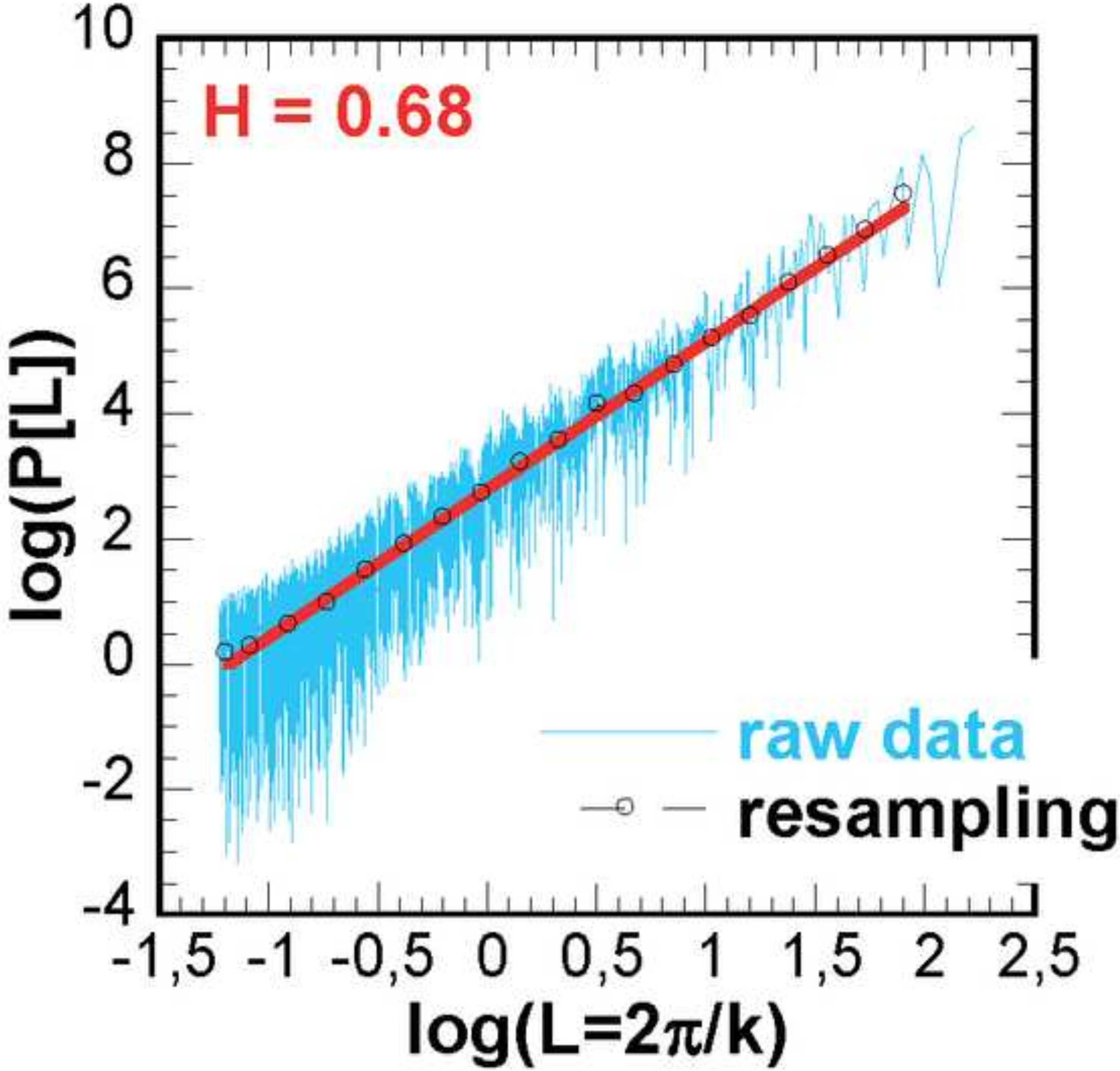

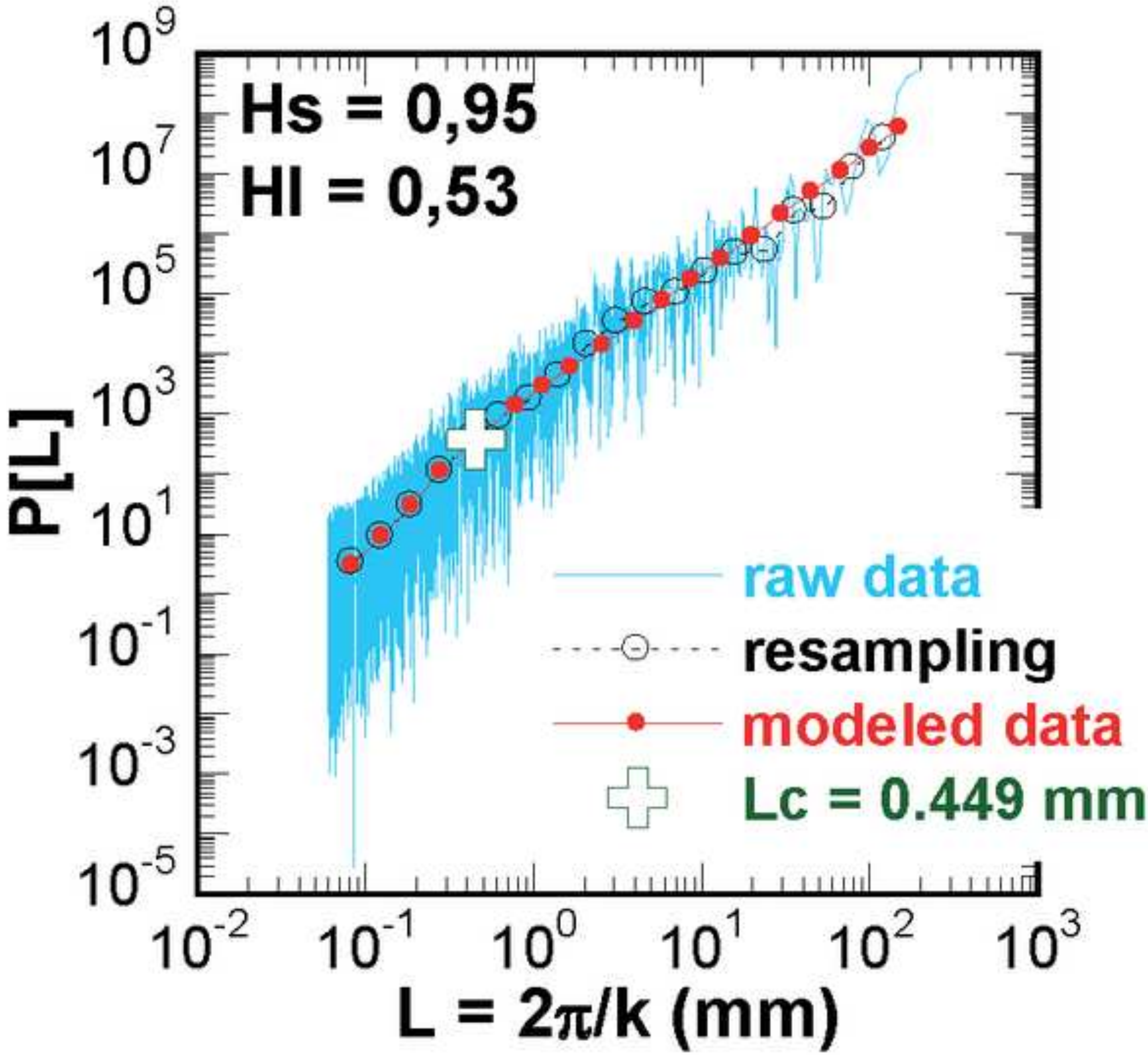
Hs = 0,95
Hl = 0,53
raw data
resampling
modeled data
Lc = 0.449 mm
P[L]
L = 2π/k (mm)
10^9
10^7
10^5
10^3
10^1
10^-1
10^-3
10^-5
10^-2
10^-1
10^0
10^1
10^2
10^3

Figure
Click here to download high resolution image

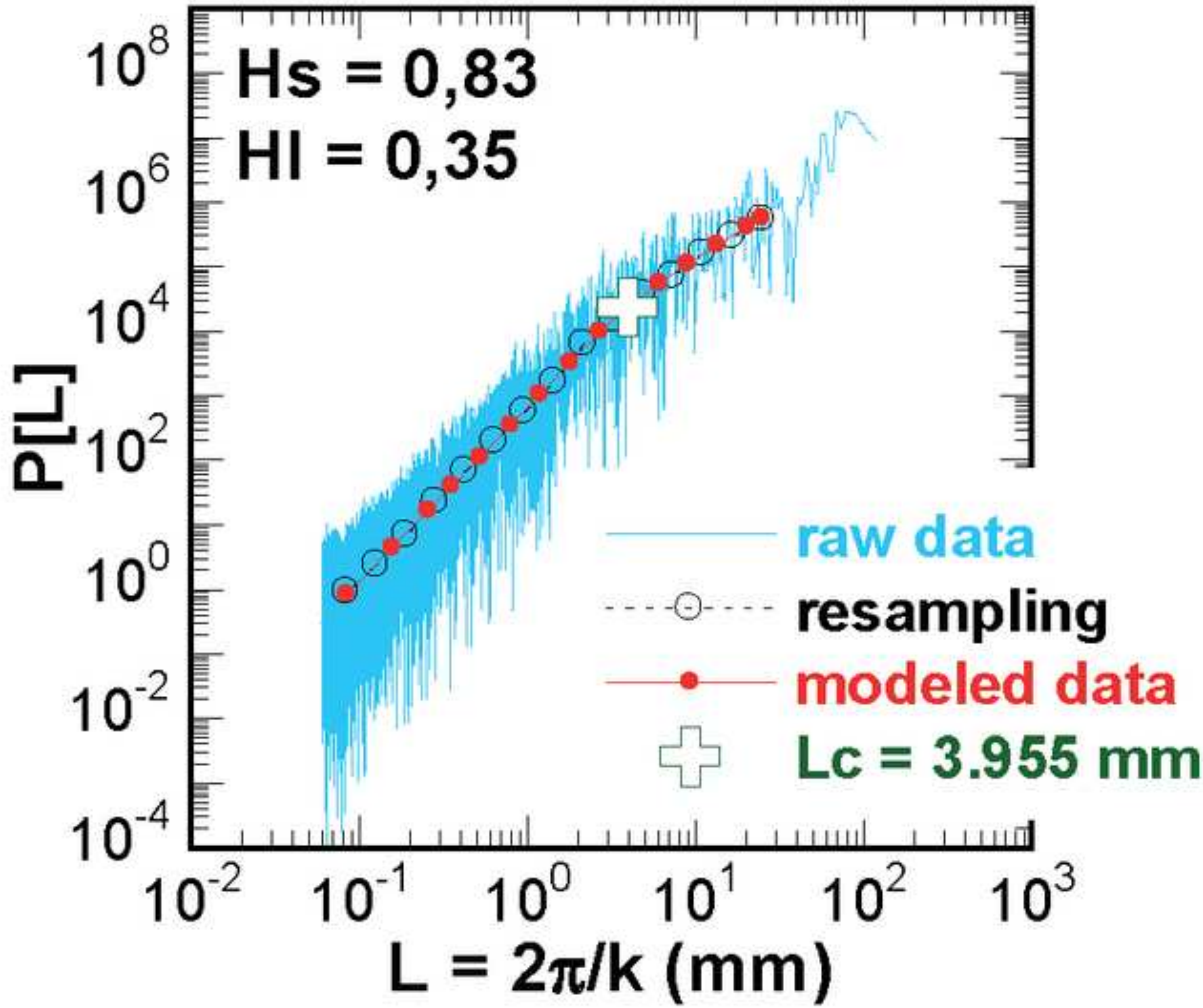

Figure
Click here to download high resolution image

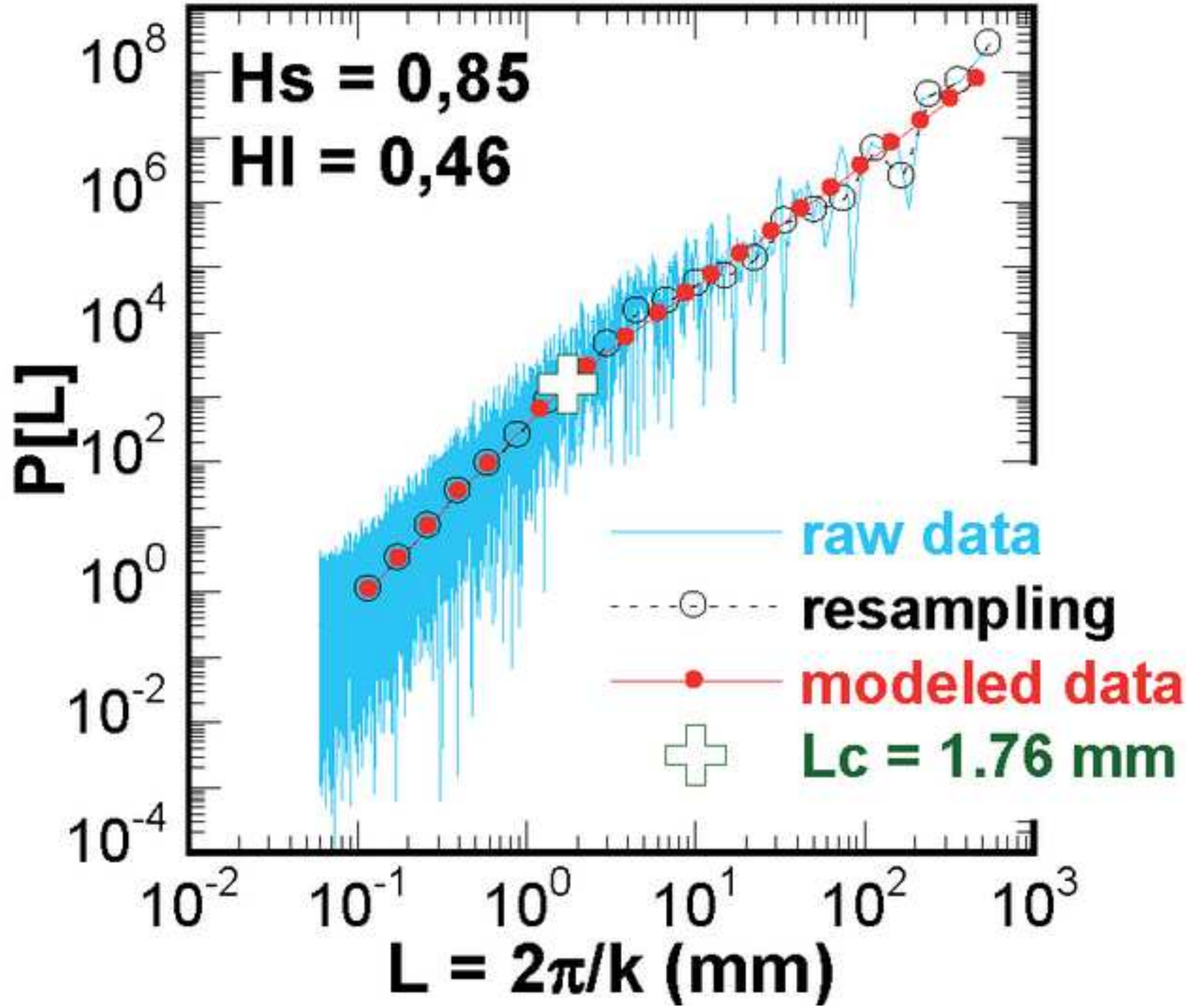

Figure
Click here to download high resolution image

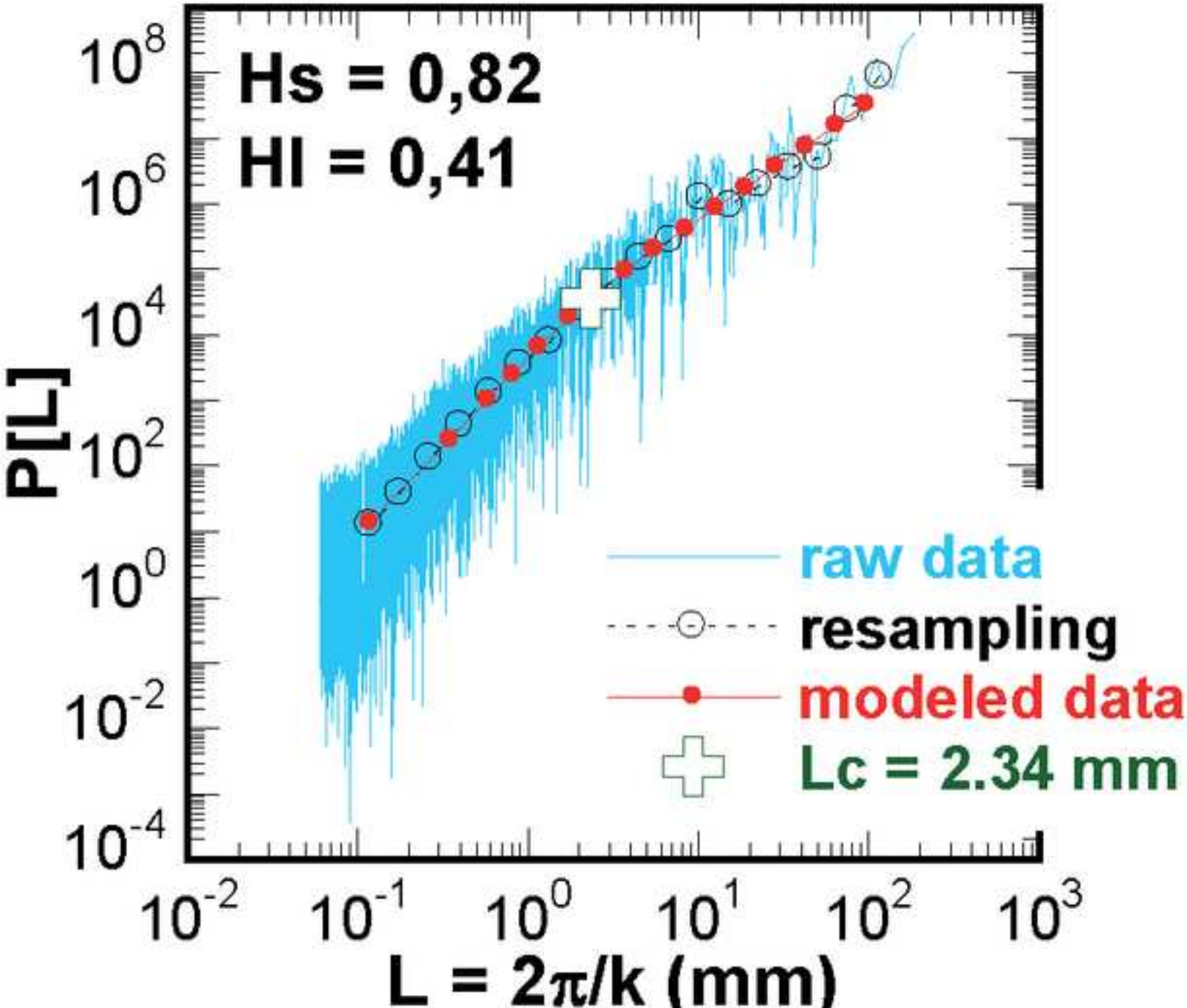

Figure

Click here to download high resolution image

Figure
Click here to download high resolution image

Figure

Click here to download high resolution image

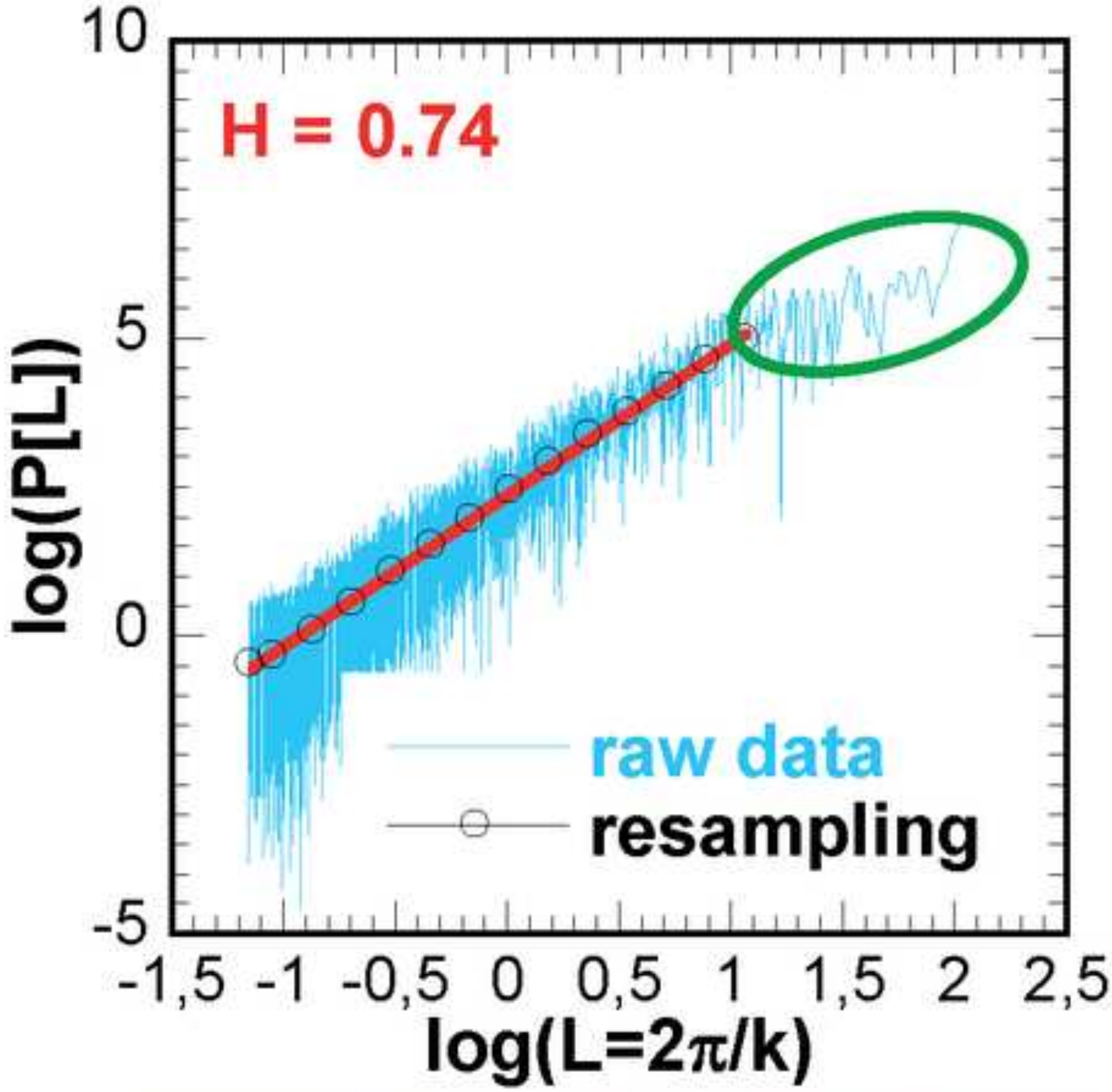

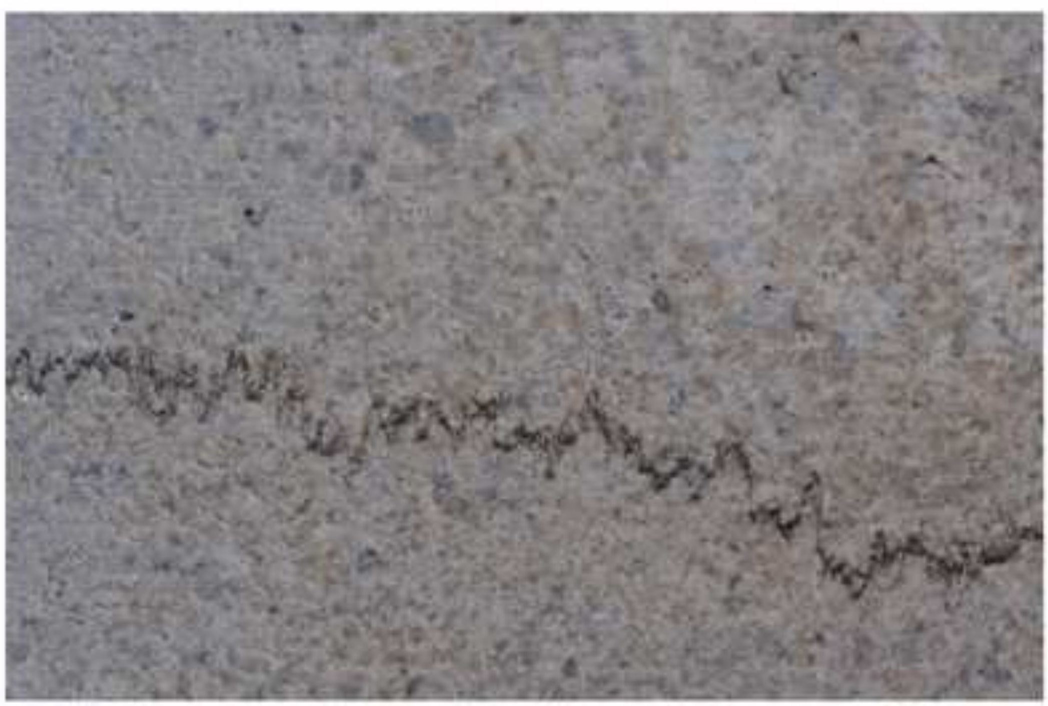

Figure
Click here to download high resolution image

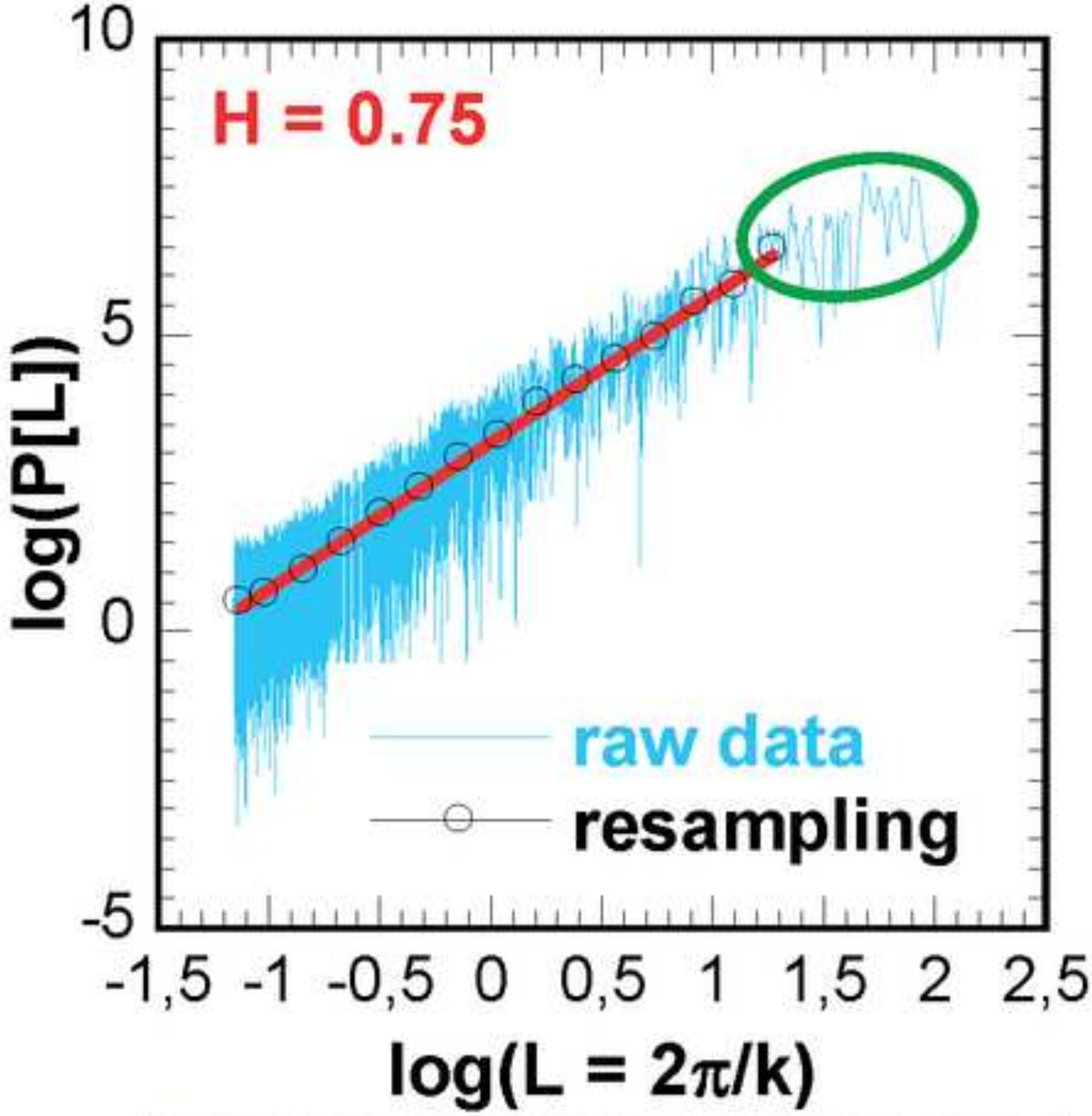

Figure
Click here to download high resolution image

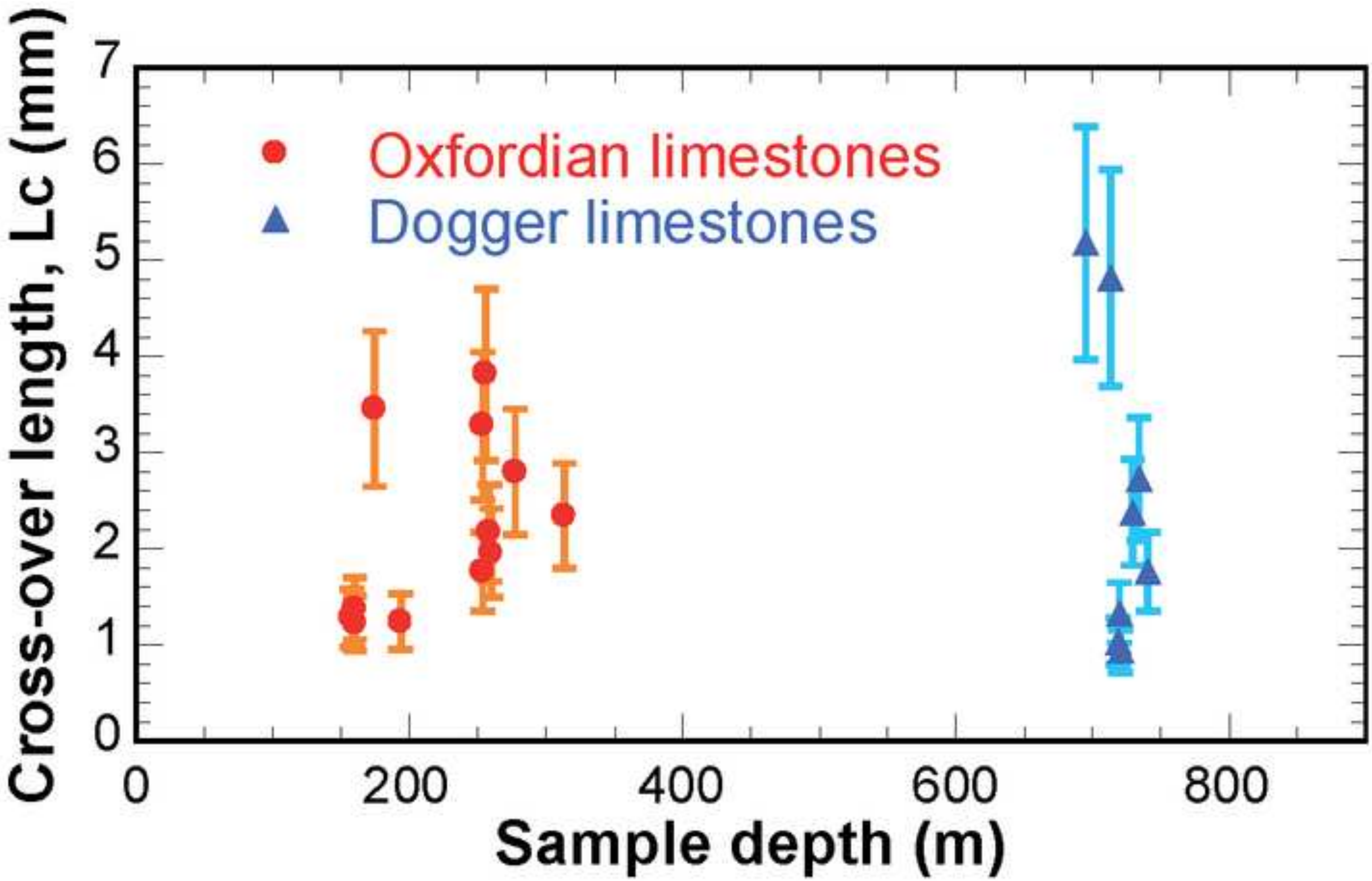

Figure
Click here to download high resolution image

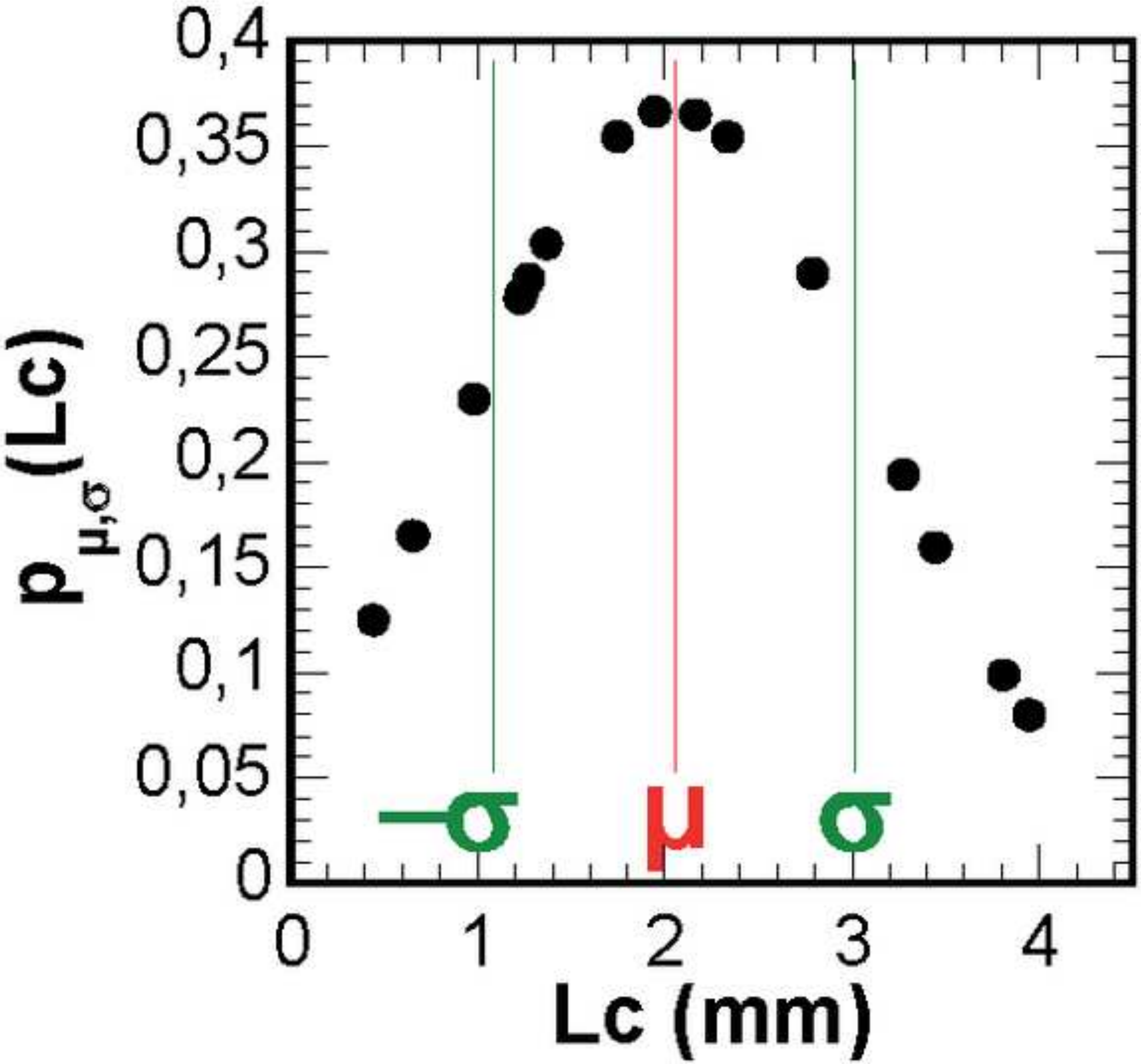

Figure
Click here to download high resolution image

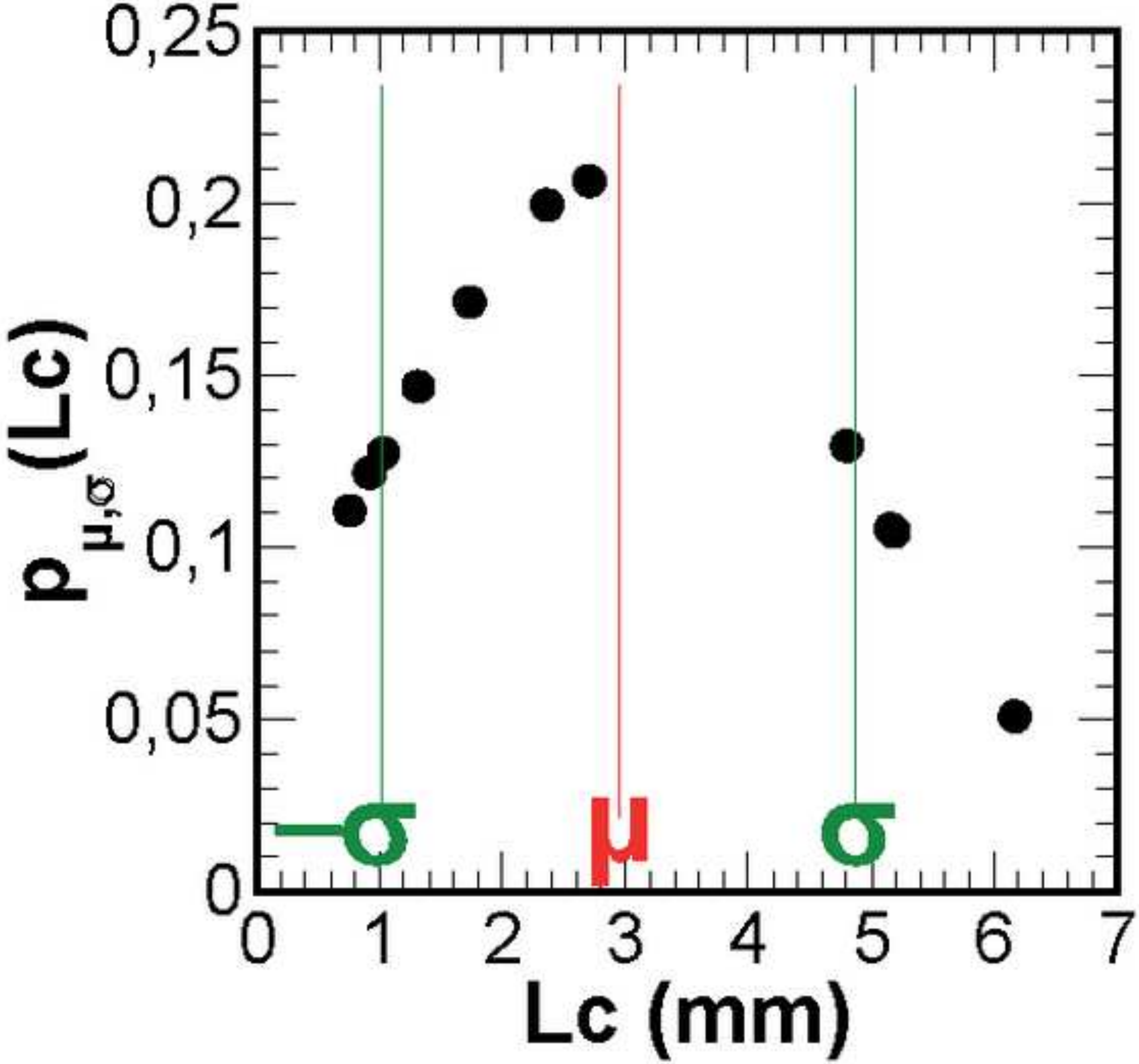

Figure
Click here to download high resolution image

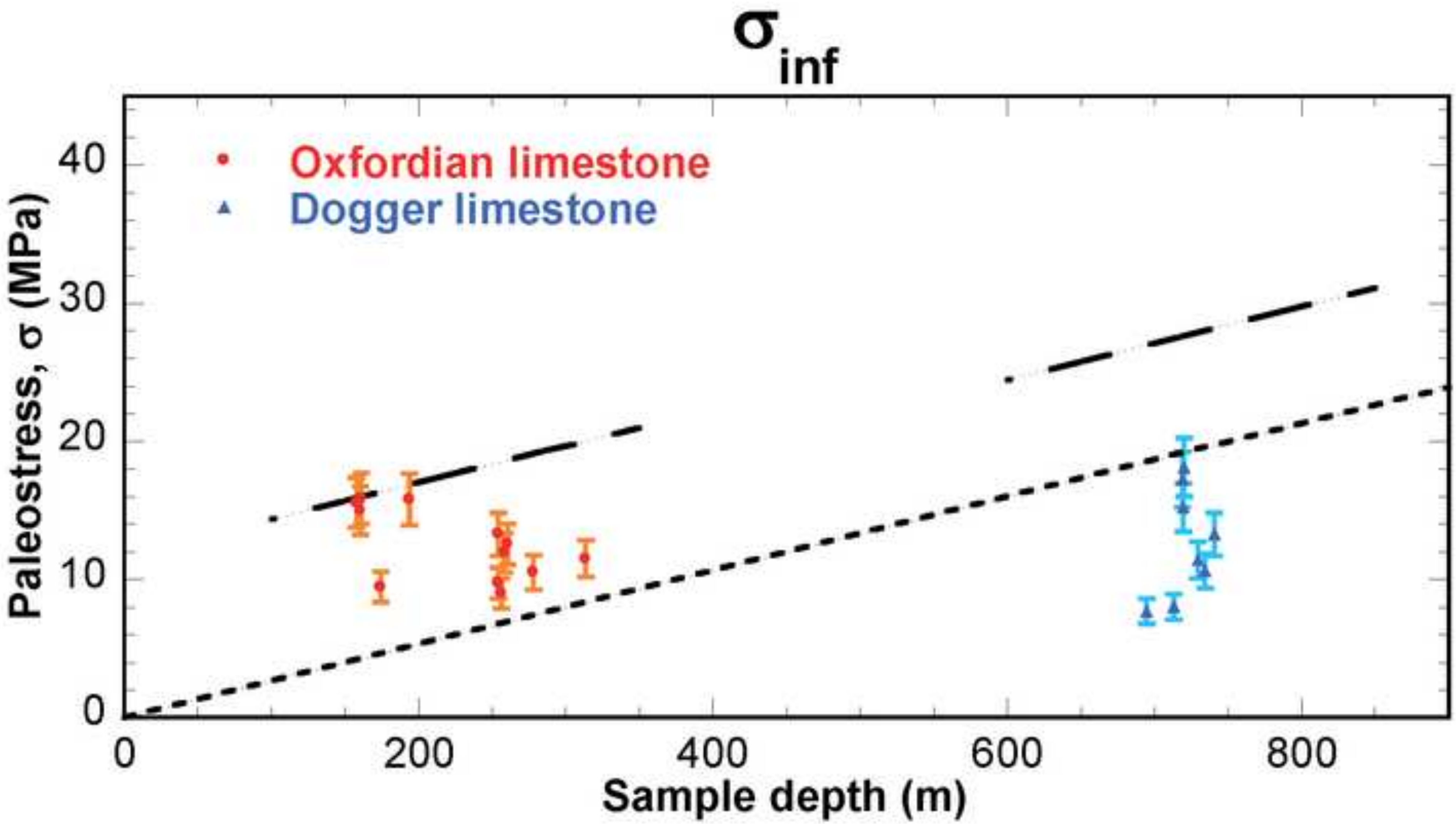

Figure
Click here to download high resolution image

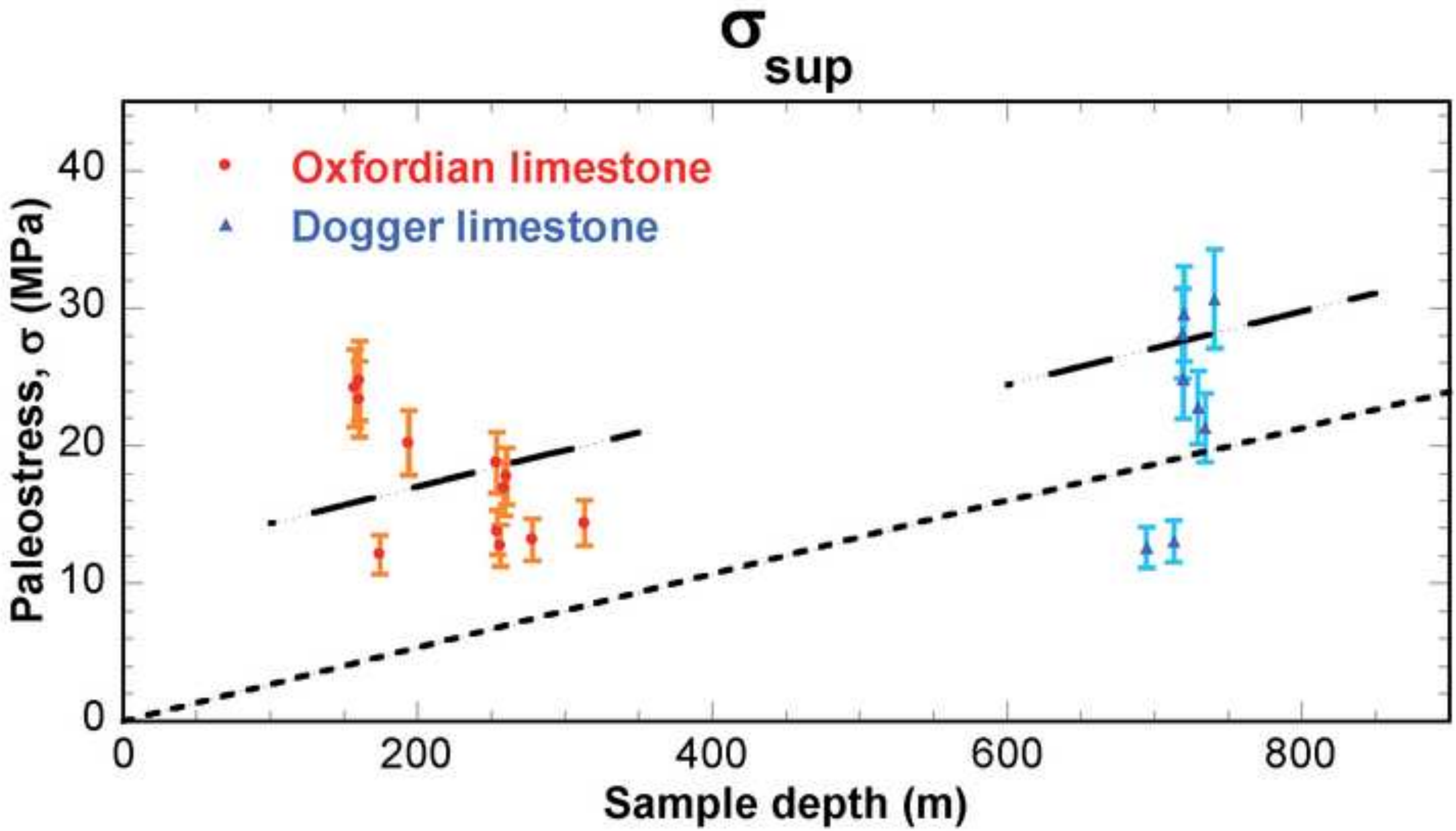

Figure

Click here to download high resolution image

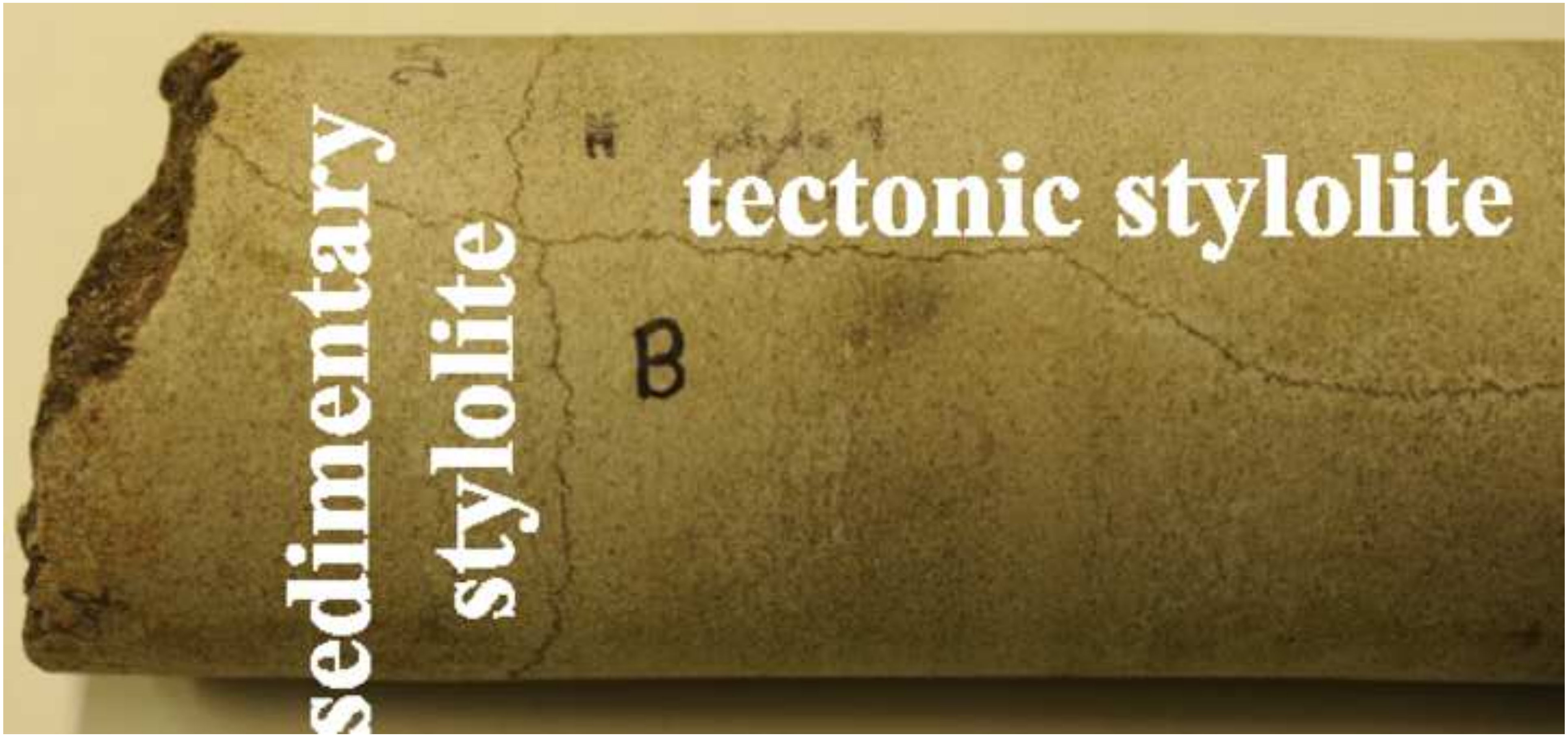

Figure
Click here to download high resolution image

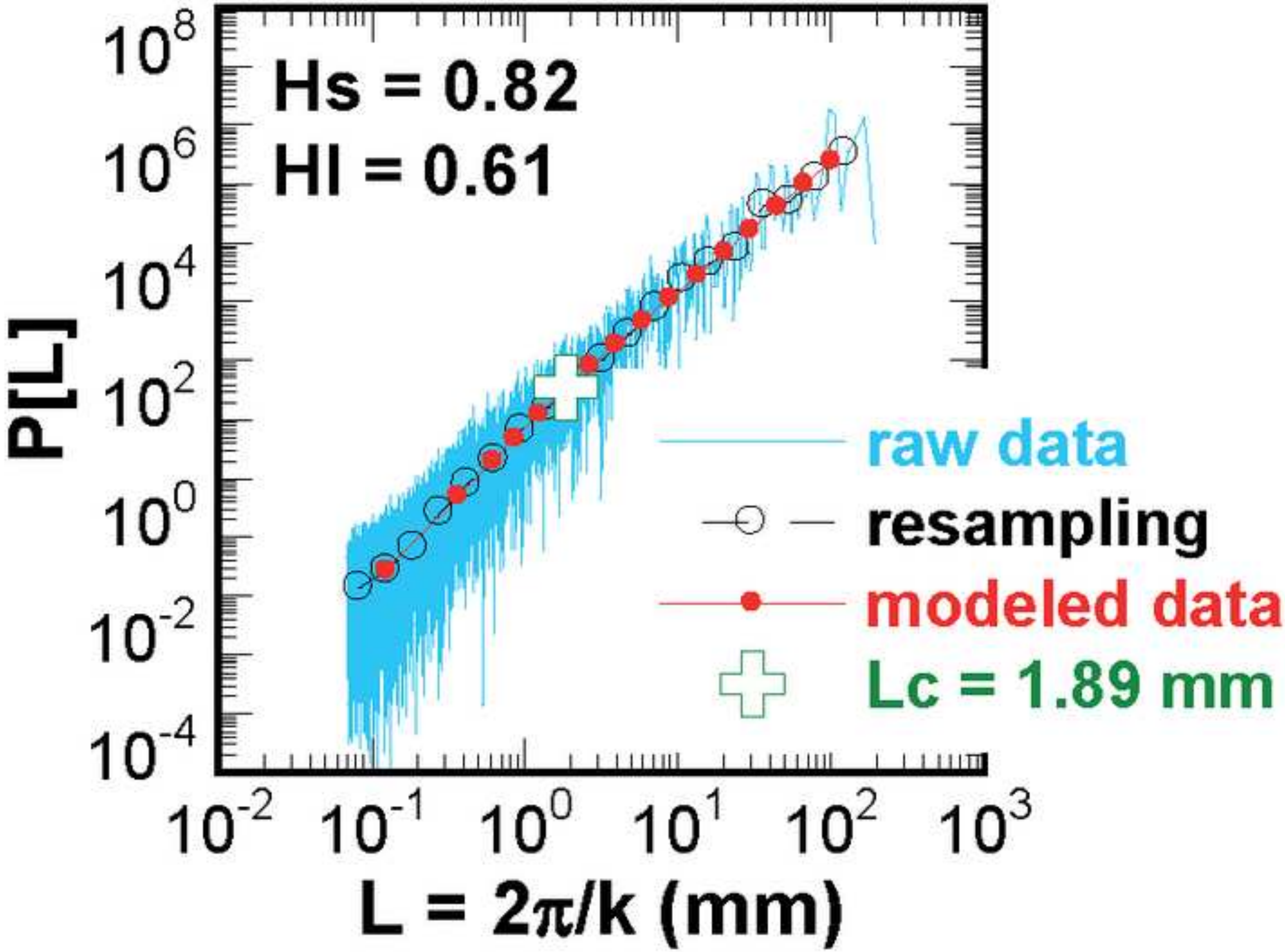

Figure
Click here to download high resolution image

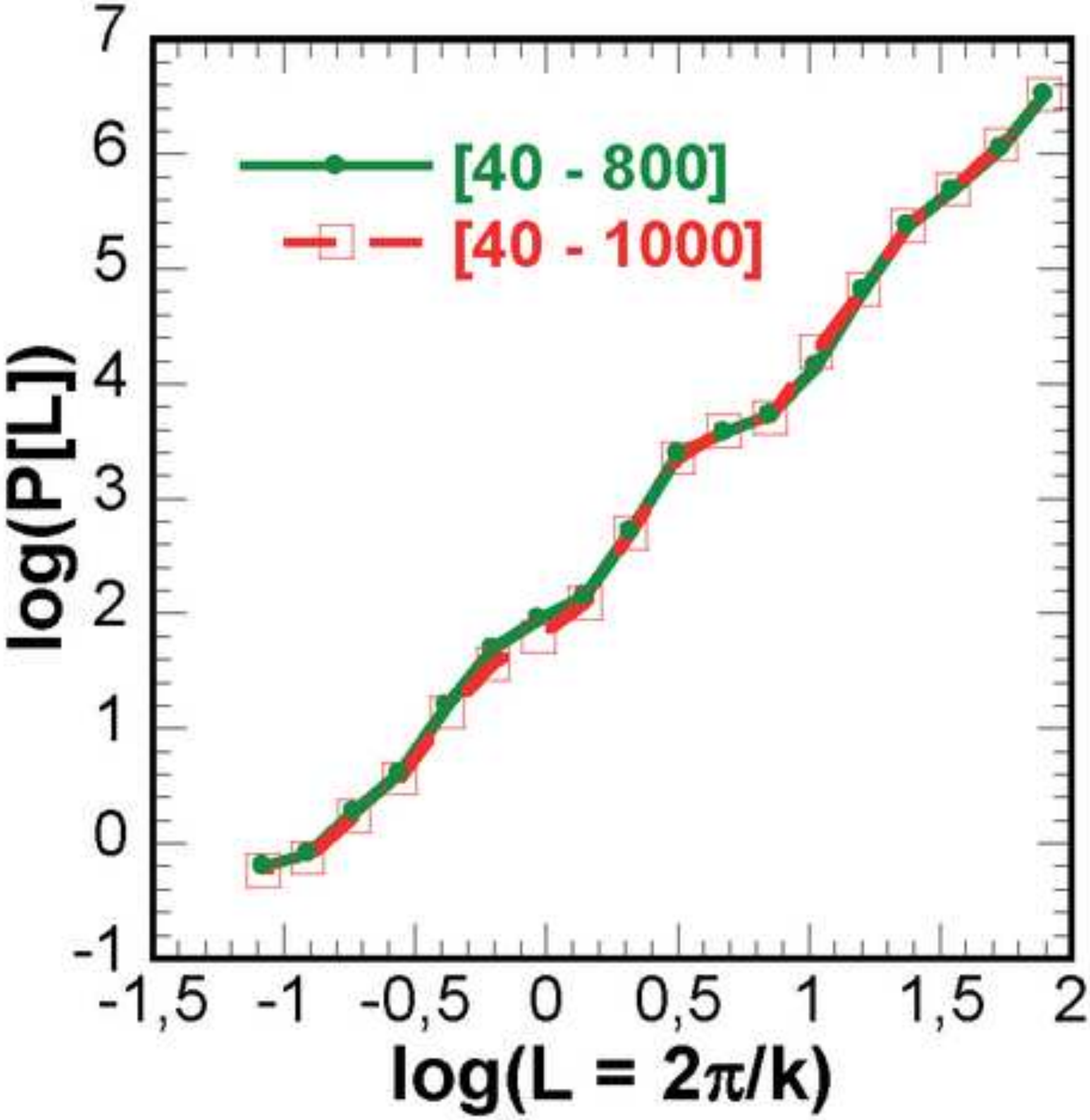

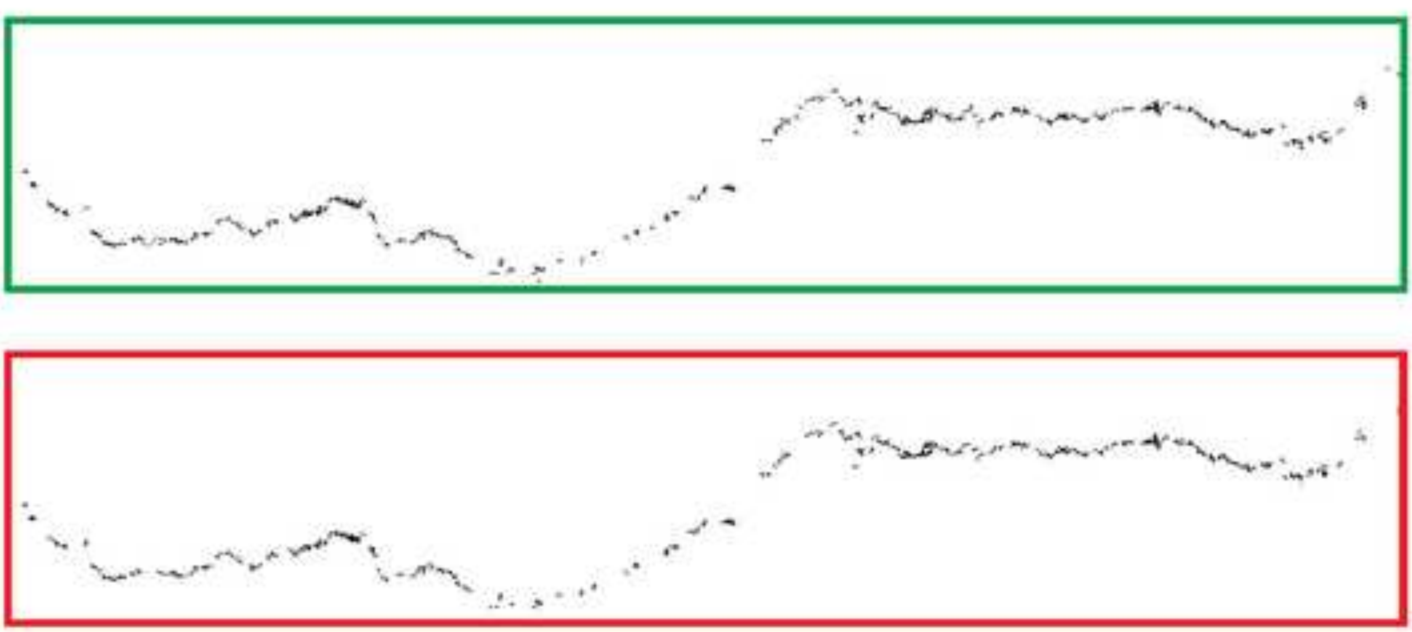

Figure
Click here to download high resolution image

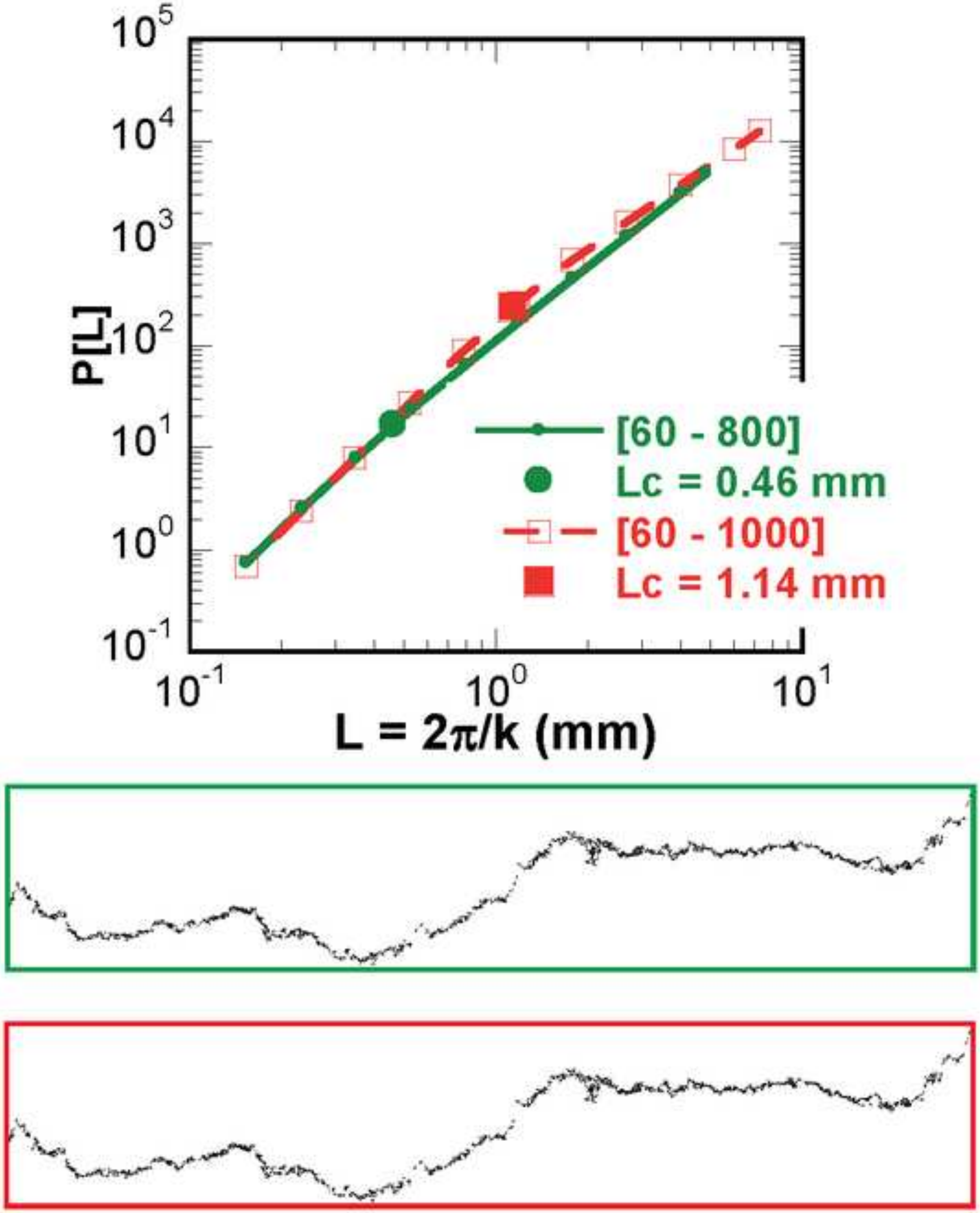

Figure
Click here to download high resolution image

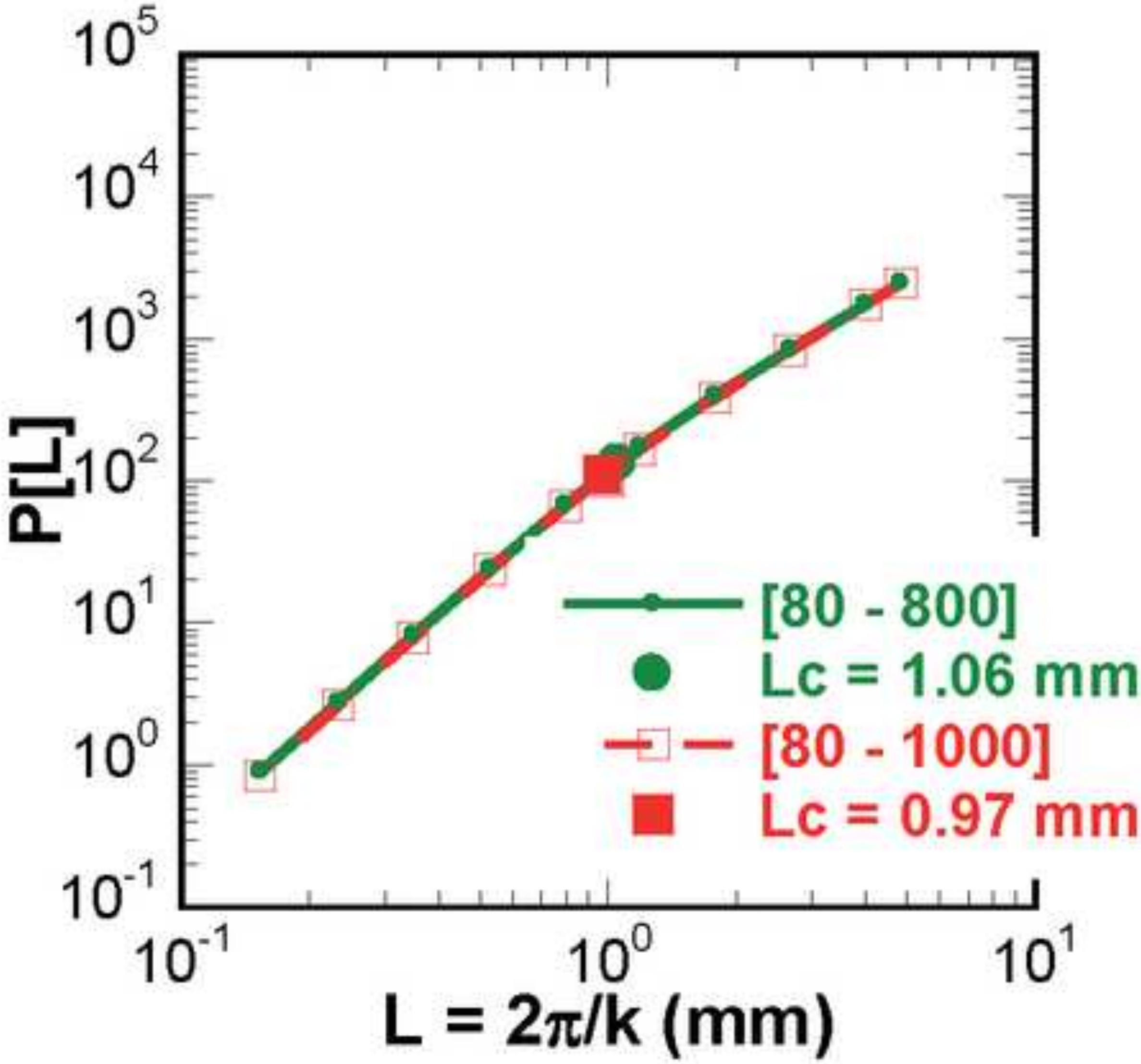

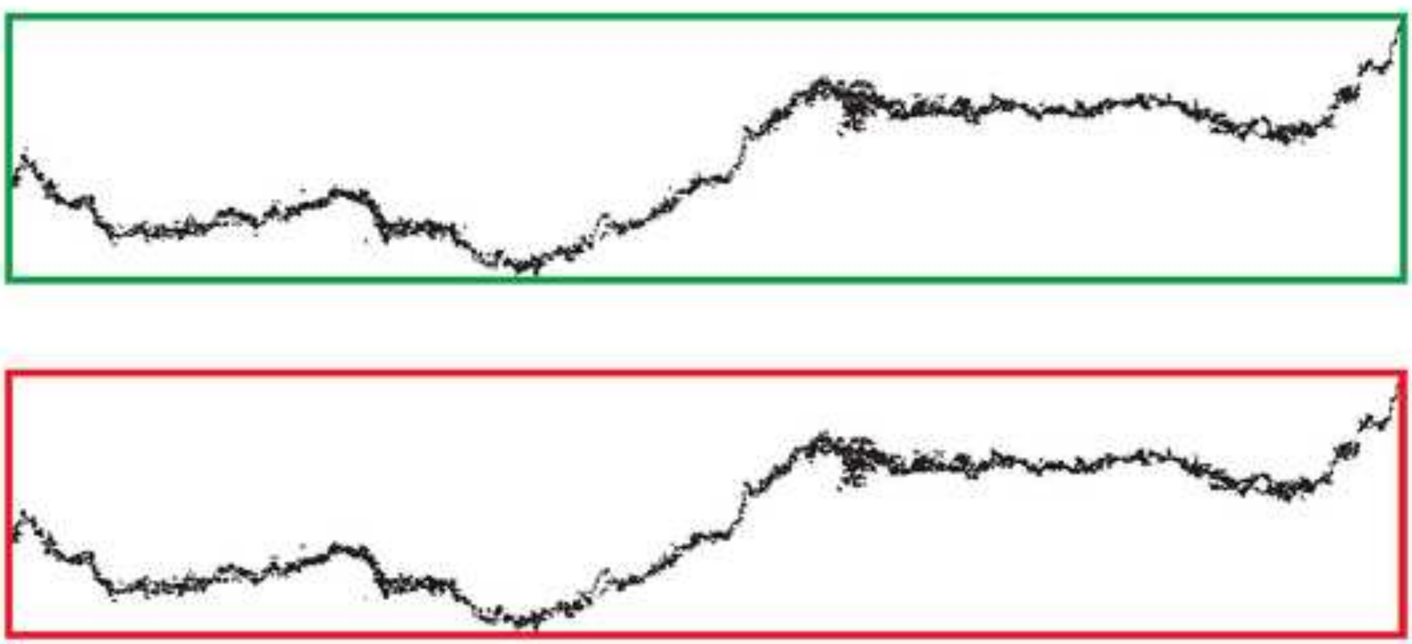

Figure
Click here to download high resolution image

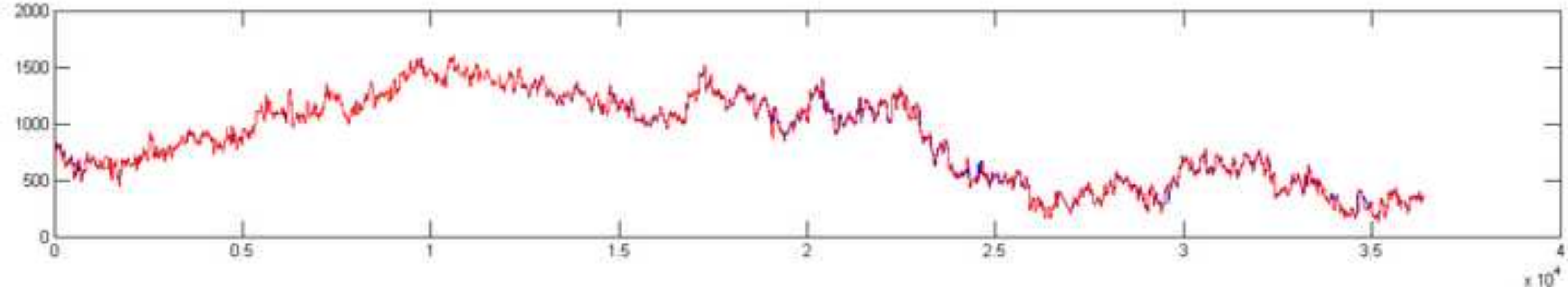

Figure
Click here to download high resolution image

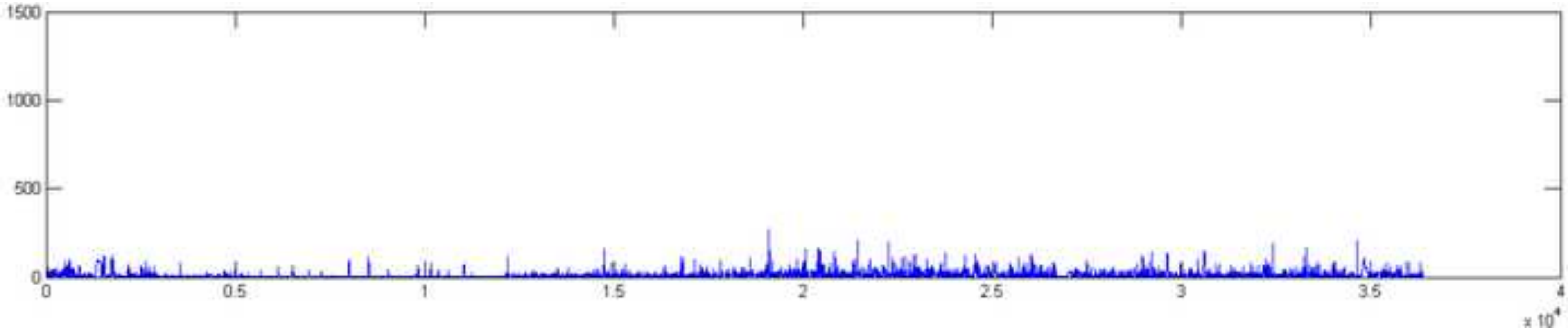

Figure
Click here to download high resolution image

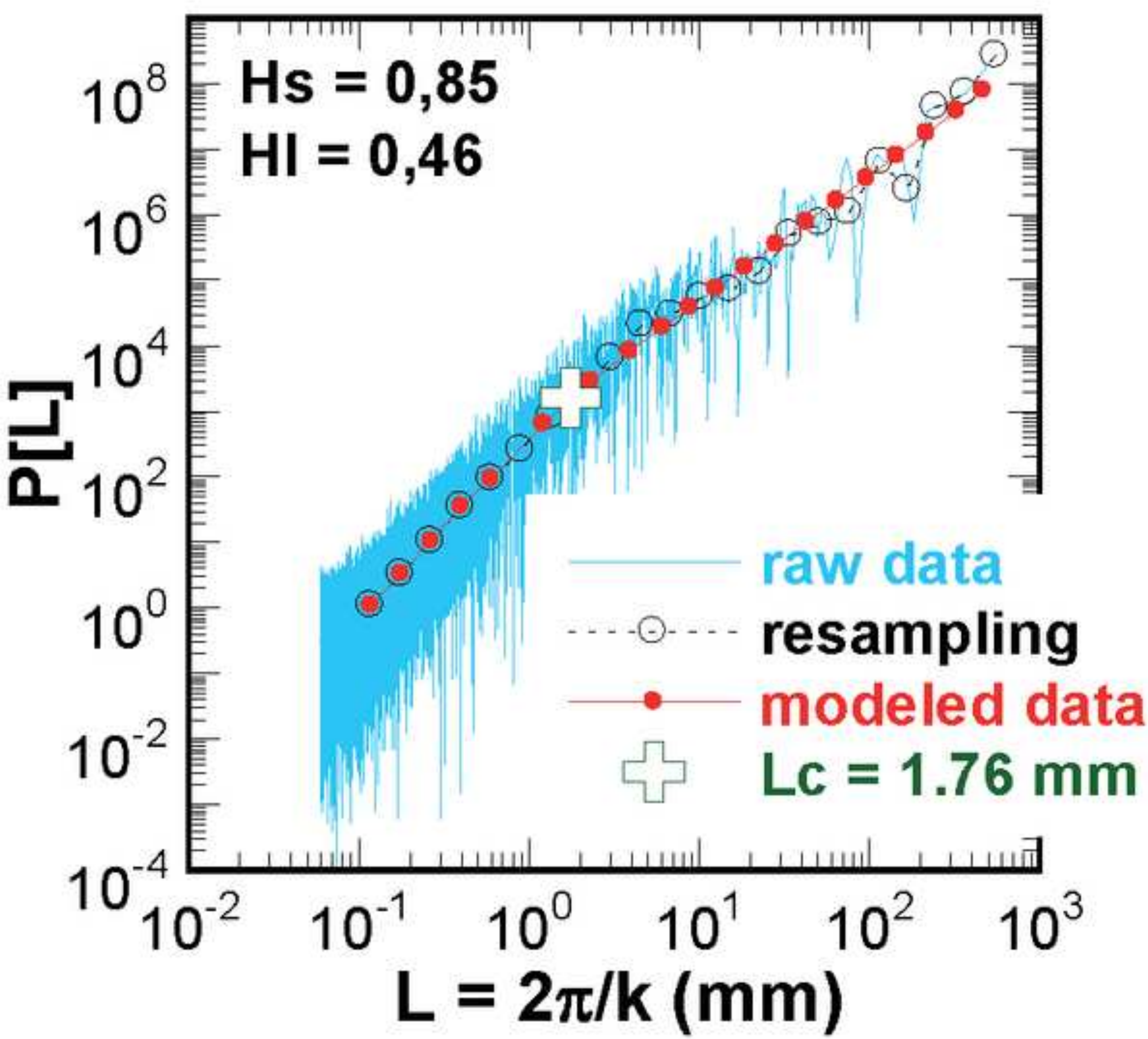

Figure
Click here to download high resolution image